PROCUREMENT EXECUTIVE, MINISTRY OF DEFENCE

AERONAUTICAL RESEARCH COUNCIL

CURRENT PAPERS

Exploratory Tests on a Forward-Mounted Overwing Engine Installation

by

D. J. Kettle, A. G Kurn and J. A. Bagley

Aerodynamics Dept., R A E., Farnborough

LONDON: HER MAJESTY'S STATIONERY OFFICE

1972

PRICE 95 p NET

EXPLORATORY TESTS ON A FORWARD-MOUNTED OVERWING ENGINE INSTALLATION

by

D. J. Kettle

A. G. Kurn

J. A. Bagley

SUMMARY

Wind-tunnel tests have been made to assess the aerodynamic potential of
an overwing installation for fan-jet engines on a typical modern transport
aeroplane. Low-speed tests on a complete model with free-flow nacelles and
tests at higher speed on a partial model incorporating a blown jet are
described; it is concluded that the lift-dependent drag associated with such
an installation would be significantly greater than that of a conventional
underwing engine installation.

CONTENTS

1   INTRODUCTION

The current generation of turbofan engines for transport aircraft have
nacelle diameters of the order of three metres, and their conventional installa-
tion on a typical transport aeroplane, on pylons beneath a swept wing, involves
a compromise between aerodynamic and other considerations which can only be
resolved after extensive testing. It therefore seems to be worth taking a
fresh look at unorthodox installations, and particularly at those where the
engine is close to the wing so that the total wetted area is reduced: these
promise a potential saving in skin friction to be set against any increased
interference drag.

Of the several possible engine locations which could be considered, this
Report is concerned with a nacelle above the wing with the engine itself
carried ahead of the wing structure and with the jet exit well ahead of the
trailing edge. It is acknowledged that the jet passing over the wing surface
could cause structural problems but it is assumed that these could be solved by
known techniques if such an arrangement proved sufficiently attractive in other
respects.

The experiments described in this Report were intended as a preliminary
study of the aerodynamic characteristics of such an installation. It was
envisaged that the jet itself would play an important part in determining the
flow around the nacelle and the adjacent wing, so the first series of experi-
ments, described in section 2, were concerned with this aspect. A jet was
blown from a suitably-shaped nozzle (representing the after-part of a nacelle
for a modern turbofan engine) over an unswept wing mounted in a wind tunnel,
and the effect of the jet on the flow around the wing was determined from
pressure measurements on the wing and from flow surveys in the jet itself. A
series of similar experiments had previously been made[4] on a rig representing
a conventional underwing nacelle.

As a result of these tests, it appeared to be desirable to make some
assessment of the overall aerodynamic characteristics of a typical engine
installation on a more complete model, so a brief series of tests was made in
a low-speed wind tunnel of a wing-fuselage model fitted with free-flow nacelles.

These tests are described in section 3 of this Report, and the conclusions from the two test programmes are summed up, with reservations, in section 4.

2   EXPERIMENTS ON MODEL WITH BLOWN JET

2.1   Experimental arrangements

This experiment was carried out during 1968 and 1969 in the R.A.E. 2ft × 1½ft transonic wind tunnel, where the facility existed for representing a jet stream from a nozzle. The investigation was concerned with the measurement of static pressures on a wing, to determine how these pressures were affected by the presence of a nozzle, with and without jet thrust. A photograph of the test rig is shown in Fig.1. In addition, total pressure traverses were made through the jet to show how the jet stream developed during its passage downstream from the nozzle. To supplement the pressure measurements, schlieren photographs were taken of the jet stream and surface oil-flow patterns on the side of the nozzle were obtained.

2.1.1   The nozzle

The nozzle, shown in Fig.2, was mounted on the end of a pair of coaxial tubes that were cantilevered from the tunnel contraction. The jet air was supplied through the inner tube to the nozzle at the same stagnation temperature as the tunnel air stream. The mass flow rate of this air was measured in a 76.2 mm (3 in) diameter pipe, by a static tapping and a pitot tube placed at ¼ of the pipe radius from the wall. The pitot pressure was also used to set up the nominal stagnation pressure at the nozzle exit, H_j, assuming a loss of 13% for the length of pipework to the nozzle. This value for total pressure loss was based on previous experiments with the same jet rig (see section 2.2.4). Suction, through slots in the outer tube of the coaxial pair (Fig.1), removed part of the excessively thick free stream boundary layer that developed (see section 2.1.4).

The nozzle exit was positioned on the upper surface of the wing at 0.315 c, with a 1.6 mm rearward facing step from the inside of the nozzle to the wing surface. The underside of the nozzle was blended to the wing with plasticene, shaped to fair into the wing lower surface before 0.20 c.

2.1.2   The wing

A twodimensional wing was used for this experiment. It was mounted across the tunnel, which had solid glass side walls and a slotted roof and floor,

giving an open area ratio of 6%. The ends of the wing butted against the glass walls, and spigots from the position of maximum thickness passed through holes in the glass and were clamped to supports outside the tunnel working section.

The boundary layer on the wing upper surface was, of course, fully turbulent within the jet stream. A sublimation technique, using acenapthene, showed that the static pressure hole at 0.02 c in the chordwise row of holes outboard of the jet (section 2.1.3) created sufficient disturbance to promote turbulence over the holes behind it. On the wing lower surface natural transition occurred at 0.5 c.

2.1.3 Static pressure measurements on the wing

One hundred and twenty pressure tubes embedded just below the surface of the wing, and laid in a spanwise direction enabled surface static pressure holes to be drilled at any desired spanwise position. The instrumentation allowed 90 pressure measurements to be made. In practice, part of the testing was done measuring 60 pressures; 42 holes around the wing were on a centre-line chord behind the nozzle, whilst the remainder were on a chord at the junction with the side of the nozzle. The wing was then removed from the tunnel and a new set of 90 holes drilled; 45 of these were outboard of the nozzle, on a chord 57.1 mm (2.25 in) to starboard of the nozzle centre-line ($y/R_n = 1.80$); 17 were on the centre-line*, and the remainder on a chord 20.3 mm (0.8 in) to port of the centre-line. To obtain measurements on a chord at two other span-wise positions, $y/R_n = 1.36$ and 2.60, the nozzle with its support tube was moved laterally across the tunnel. Fig.3 shows the position of the pressure holes that were of most interest, together with a table of tunnel and jet conditions at which measurements were taken.

2.1.4 Test conditions

The range of test conditions is given in Fig.3. At all tunnel Mach numbers (M_o) free stream stagnation pressure was fixed at 67 kN/m^2 (1400 lb/ft^2), giving a Reynolds number, based on wing chord, of 1.18×10^6 at the lowest Mach number of 0.60 and 1.35×10^6 at the highest Mach number of 0.74. The wing incidence was fixed, giving lift coefficients for the wing alone of 0.316

---

* This enabled a limited number of centre-line pressures to be repeated, to check that on reinstalling the wing and nozzle in the tunnel geometric conditions were the same as before.

and 0.324 at the lowest and highest Mach numbers respectively. The stagnation pressure of the jet was varied from the free stream value to 2.98 times the free stream static pressure (i.e. from $H_j = H_o$ to $H_j = 2.98\ p_o$). The former was selected as a basic condition, giving zero thrust, to simulate a free flow nacelle as used in conventional model testing. Interest has been focussed on $M_o = 0.74$ and $H_j = 2.4\ p_o$, since these values represented typical cruise conditions for the unswept wing. At this Mach number sonic velocities were experienced over a small region of the wing alone (see Fig.4; $C_p^* = -0.626$), and the jet pressure ratio is representative of a large 5:1 by-pass ratio fan jet engine.

With the wing spanning the tunnel, Ref.1 predicted a correction $\Delta M = -0.02$ to the tunnel Mach number (M_o). This implies that the conditions mentioned above and the pressure coefficients given in the results, which are a function of M_o, should be similarly corrected. However, no corrections have in fact been made, since the conclusions drawn from the results do not depend on the precise Mach number; in any case, the tunnel corrections with the jet blowing are quite unknown.

Part of the boundary layer developed along the nozzle support tube was removed by suction through slots around the circumference of the tube. A complete description of the boundary layer suction system, which includes measurements of boundary layer thicknesses, is given in Ref.2. Recent modifications to the bends in the suction ducts increased the suction mass flow by 30%. Estimates based on this increased suction together with the results of Ref.2 give displacement and momentum thicknesses of 1.68 mm (0.066 in) and 1.25 mm (0.049 in) respectively around approximately 50% of the support tube at the connection to the nozzle. Ref.2 shows that local reductions to these thicknesses occur on the starboard side of the tube, and to a greater degree on the port side, possibly as a consequence of small cross flows.

2.2   Experimental results

The effect on the wing pressures due to jet blowing is, for convenience, presented in two stages. The part of the wing to which the jet stream was attached is considered in detail, as large pressure changes and drag effects occurred in this region. The spanwise interference outside the jet stream is then examined, and the two regions combined in an overall lift analysis.

Finally, the development of the jet stream, during its passage downstream from the nozzle, is discussed.

2.2.1 Interference on the wing within the jet stream

Fig.4 shows that (as would be expected) the presence of the nozzle at zero thrust gives an appreciably different pressure distribution, on the centre-line chord ($y/R_n = 0$) behind the nozzle exit, from that on the wing alone. With the jet blowing there is no significant change to the lower surface distribution, but on the upper surface large pressure gradients occur due to the expansion waves and compression shock waves within the jet.

Measurements made at $y/R_n = 0.8$ (not presented) showed that at zero thrust the pressures were slightly less on the upper surface between 0.4 c and 0.6 c than those at $y/R_n = 0$. With the jet blowing there were insufficient pressure measurements to define the distribution clearly. It appeared that the pressure distribution was similar to that on the centre-line with a slight dis-placement in the upstream direction.

Pressure distributions on the upper surface of the wing along the centre-line, as jet pressure increases from zero thrust, are shown in Fig.5, with corresponding schlieren photographs in Fig.6. It will be noted that shock waves are visible in the jet stream at a value of jet pressure ratio $H_j/p_o = 1.73$, when the jet velocity is expected to be entirely subsonic. However, the pressure on the upper surface of the wing at the exit position is appreciably less than the free stream value, so a supersonic jet is possible at this condition.

The pressure drag increment due to jet flow, obtained by integrating the upper surface pressure distributions of Fig.5, without considering skin friction, is shown in Fig.7. It can be seen that at $M_o = 0.74$ with jet pressure ratios greater than 2 the drag on the surface of the wing swept by the jet stream has more than doubled. As jet pressure ratio increases the pressure drag increment shows an oscillating trend as the jet pattern expands downstream and successive shock cells pass over the trailing edge. A similar tendency was observed in N.G.T.E. tests of a somewhat similar configuration in a static environment[3]. The drag values obtained at these higher jet pressures are not very accurate since the pressure distribution is not well defined near the trailing edge, where the surface slope is greatest. An estimate of the possible errors in the results of these drag integrations is shown at the two highest jet pressure ratios for alternative pressure distributions near the trailing edge (Fig.5).

At a free stream Mach number of 0.6 the values of the pressure coefficients on the wing, with jet blowing, are appreciably larger than at $M_o = 0.74$ (cf. Figs.4 and 8). This suggests that the free stream total head is not the most appropriate choice of nondimensionalising parameter; it is to be expected that the pressures on this part of the wing will depend mainly on the air velocity inside the jet rather than on that in the free stream. At $M_o = 0.6$ the ratio of jet velocity to stream velocity is about 20% higher for a given value of jet pressure ratio than it is at $M_o = 0.74$.

To demonstrate this more clearly, pressure distributions at a fixed value of jet pressure ratio and various stream Mach numbers have been plotted in Fig.9 as a fraction of free stream static pressure p_o*. Schlieren photographs at the two extreme Mach numbers $M_o = 0.6$ and 0.74 are also given in Fig.10. It is clear that, in general, the free stream Mach number has little effect on the wing pressures. There is a slight downstream expansion of the cell pattern in the jet as M_o increases, similar to the effect produced by slightly increasing jet pressure ratio at a fixed Mach number (cf. Figs.6 and 10). The most noticeable change is between 0.6 c and 0.8 c (Fig.9) where the character of the distribution is altering. The peak pressures are also changing slightly.

Since the ratio of jet velocity to free stream velocity increases as Mach number is reduced it is to be expected that the jet-dependent drag increment also increases with decreasing Mach number. The integrated pressures of Fig.9, presented in Fig.11, show this to be so. For $M_o < 0.64$ the drag increment due to jet flow, on the upper surface of the wing behind the nozzle, is more than twice the basic drag at zero thrust.

The lift increments, corresponding to the drag increments of Figs.7 and 11, are plotted in Fig.12a. For a given jet pressure ratio or Mach number change the incremental change in lift is smaller than the incremental change in drag. The lift must vary with jet pressure ratio in a similar way to the drag; a line is drawn through the points in Fig.12a to indicate this but it is of course purely speculative. The lift results are modified and presented in Fig.12b as $\bar{p}_j/H_j$, where $\bar{p}_j$ is the mean pressure acting on the wing behind the nozzle; they almost collapse onto a single curve regardless of free stream Mach number.

---

* p_o is a more convenient choice of nondimensionalising parameter, at a fixed value of H_j/p_o, than the jet total head H_j itself, simply because there is a variation of H_j across the nozzle exit - see Fig.19.

A line representing p_o/H_j is drawn on the figure for comparison, and it can be seen that $\bar{p}_j/p_o$ is only slightly greater than 1. For $H_j = H_o$, $\bar{p}_j/p_o = 1.04$ at $M = 0.60$ and 1.08 at $M_o = 0.74$; with $H_j = 2.4\, p_o$, $\bar{p}_j/p_o = 1.10$ and 1.135 for the same Mach numbers.

2.2.2 Interference on the wing outside the jet stream

Figs.13 to 18 show the interference effect of the nozzle, with and without jet blowing, at three spanwise positions for two free stream Mach numbers. The most significant feature of these pressure distributions is the increase in pressure on the upper surface, commencing at about 0.1 c, which reaches a maximum just downstream of the nozzle exit. Within this region the pressures are hardly affected by jet pressure ratio. The distribution on the wing close beside the nozzle (not presented) was very similar to that at $y/R_n = 1.36$, except that the velocity increased just before the nozzle exit, presumably because of an entrainment effect due to the proximity of the jet stream. The figures show that further downstream the distributions are affected by jet blowing, higher velocities being induced when the jet pressure ratio is 2.4. The internal divergence of the nozzle shape in the spanwise direction (Fig.2), producing outflow at the exit, is probably the cause of the 'trough' in the pressure distributions.

2.2.3 The effect of the jet on lift

The pressure distributions discussed in the previous two sections, have been integrated to produce the spanwise lift variation with respect to the lift of the wing alone in Fig.19.

Both for the wing alone and with the nozzle present, the lift within the spanwise width of the nozzle has been measured over the last 65% of the chord only, since no pressures were measured ahead of this on the nozzle or on the fairing under the wing. Hence the figure shows that behind the nozzle exit the lift at 'cruise' conditions ($M_o = 0.74$ and $H_j/p_o = 2.4$) is comparable with that of the wing alone. At the same jet pressure ratio, but with the Mach number reduced to 0.60 there is an increase in lift of about 27%. An increase in lift is to be expected since on the wing upper surface the jet flow velocity increases with respect to free stream velocity as Mach number is reduced (see section 2.2.1). With zero thrust there is a loss of lift of about 35-40% at both Mach numbers.

10

Outboard of the nozzle one would expect the lift increments to tend to zero as $y \to \infty$; the lift curves at $M_o = 0.60$ look reasonably sensible, but those at $M_o = 0.74$ are not so convincing. The only repeat measurement made was at $y/R_n = 1.80$ for $H_j/p_o = 2.4$, which gives a lift value somewhat larger than the original (see figure)*. A rough estimate of the experimental scatter is shown by the cross-hatched bands on Fig.19. Although the results are thereby degraded to some extent they nevertheless give information to a sufficient degree of accuracy to be worth noting. For both cases, with and without thrust, the lift does not change greatly with free stream Mach number. At zero thrust there is a loss of lift of about 20 ±5% at $y/R_n = 1.5$ and 10 ±5% at $y/R_n = 2.75$. With thrust ($H_j/p_o = 2.4$) there is no loss of lift, and possibly a slight gain. It should be noted that the increase in lift, achieved by jet blowing, is concentrated on the upper surface of the wing over the last 50% of the chord for short spanwise distances outboard of the jet stream (see Figs.13 and 14). This increase in lift may well be due, in part, to the formation of a vortex on each side of the jet (see section 2.2.4).

2.2.4 Development of the jet stream

Pitot measurements across the jet stream at $H_j/p_o = 2.4$ for the two extreme Mach numbers of the test, $M_o = 0.60$ and 0.74, are presented in Figs.20 to 22 as contours of constant pressure.

The nominal jet pressure ratio, $H_j/p_o = 2.4$, at which these traverses were made, give $\Delta H/H_o$ values of 0.88 and 0.67 for the free stream Mach numbers of 0.60 and 0.74 respectively. At the nozzle exit (Fig.20) it can be seen that there is an appreciable pressure gradient across the jet, and although the mean stagnation pressures have not been calculated, inspection of the pressure contours indicate that the nominal values of jet stagnation pressure (H_j), derived by the method given in section 2.1.1, are reasonably accurate. Thickening of the boundary layer on the top surface of the nozzle is apparent, and the closed loops near the top corners suggest vortex flow. This vortex flow is corroborated by the oil flow photograph of Fig.23**, which shows considerable upflow on the side of the nozzle towards the sloping upper surface.

---

* It is worth mentioning that a repeat measurement made within the jet stream gave an identical answer.

**The vertical marks just upstream of the wing leading edge, and the apparently thickened oil region around the shoulder at the circular section, are due to file marks, not to any flow phenomena.

The internal geometry of the nozzle, diverging in a spanwise direction (Fig.2), must produce an outflow which is further conducive to vortex flow. At the wing trailing edge (Fig.21) the divergent flow is apparent by the increase in width of the jet stream. The jet has also curled up quite appreciably at the ends, suggesting the development of large vortices. Further downstream, at 0.92 c behind the wing trailing edge (Fig.22), the flow has developed a stage further with the breakdown of the jet into two separate cores although it does not seem to have widened appreciably. There have been several experimental measurements of jet development in a cross-flow where a similar rolling-up and splitting of the jet sheet has been observed, and it seems probable that the development of this jet is due mainly to the downwash field of the lifting wing. On the other hand, it appears from some preliminary experiments which were made with an elliptic nozzle that a non-circular jet can deform in a rather similar fashion with little or no cross-flow to provoke it (Fig.24).

3   COMPLETE MODEL EXPERIMENTS

3.1   Description of model

The basic model used for the tests in the No.1 $11\frac{1}{2}$ ft low-speed tunnel comprised a fuselage mounted on a swept-back wing representative of present-day 'airbus' configurations as shown in Fig.25. The tests were made without either fin or tailplane. The model has been used in a variety of investigations[5,6] and is described here only briefly. The wing had a quarter-chord sweep-back angle of 25°, aspect ratio 8, a taper ratio of 3:1 and thickness/chord ratio of 0.11; the wing section was R.A.E. 100 (symmetrical), the wing span, 2.032 m (6.667 ft), and gross area, 0.5162 m^2 (5.556 sq ft). The leading edge was hinged on the lower surface at $12\frac{1}{2}$% chord over the complete span, so providing a drooped section for high-lift in conjunction with a trailing edge single-slotted Fowler-type flap extending from 10% to 65% of the gross semi-span. The fuselage, the central portion of which was cylindrical had a diameter of 0.305 m (12 in), giving a diameter/wing root chord ratio of 0.89. It was mounted with the wing in a mid-low position with a wing/body angle of $3\frac{1}{2}^{\circ}$.

Two pairs of overwing nacelle units were tested, types A and B, as shown in Figs.26 and 27. They had the same circular intake cowl, with a throat diameter of 114 mm (4.5 in); nacelle A had a nozzle shape which is scaled up from the nozzle used in the 2ft × $1\frac{1}{2}$ft tunnel tests, whilst nacelle B was flared in plan view to produce an exit with the same area as nacelle A but a smaller height. (Such a nozzle shape on a full-scale aircraft might be expected to be quieter than that of nacelle A.) The longitudinal position of the intake was

12

the same as that of a pylon-mounted nacelle (Fig.28), a pair of which had
previously been tested on the same model. The latter nacelle units were based
on a version of the RB 178 with a by-pass ratio of 4. The internal lines of
the overwing nacelles were made as simple as possible and the intake (throat)
area was the same as for the underwing nacelles. The ratio of exit/intake area
for the underwing nacelles was 0.786 and for nacelles A and B it was 0.616*.
Both types of nacelle were positioned at the same spanwise station, with the
engine centre-line at 30% of the gross semi-span; this position is somewhat
closer to the fuselage than on current airbus designs. The height of the over-
wing nacelle centre-line above the wing plane for nacelles A and B was 0.13 and
0.10 of the local wing chord respectively; for the underslung nacelles, the
centre-line was 0.32 of the local chord below the wing plane.

3.2   Test details

The tests consisted of measurements of lift, drag and pitching moments on
the plain wing and body, with and without nacelles. The effect of the nacelles
on the overall forces and moments was also investigated with drooped wing lead-
ing edge and trailing edge flaps deflected to simulate both take-off and landing
configurations. Flow through the nacelles was allowed to occur naturally and
measurements with a rake of pitot and static tubes in the intake showed that the
ratio of mean velocity (V_t) at the throat/free stream velocity (V_o) varied from
about 0.53 at zero wing incidence to about 0.61 at 9°. These values are about
20% lower than the estimated full-scale values, suggesting that the external
flow at the intake lip was somewhat non-representative of full-scale, but this
discrepancy is not thought to invalidate the results. The measured value of
V_t/V_o for the underslung nacelles was 0.9 and did not vary with wing incidence
significantly. A more important consequence of the 'free-flow' technique used
in the complete model test, is that the full-scale jet exit conditions are not
simulated. The extent to which the lift, drag and pitching moment measurements
may be affected by the jet efflux may be small for conventionally situated
underslung nacelles, but for overwing nacelles exhausting directly over the wing
upper surface, the interference may be more marked. In the discussion of the

---

* Where the intake area is defined as the area at the throat; the corresponding
  values based on highlight area are 0.650 and 0.509 for the underwing and
  overwing nacelles respectively.

results which follows, the effects of the 'free-flow' nacelles on the overall forces and moments are described; and reservations about the effects of a lack of jet representation are discussed in the conclusions.

The tests were made in the No.1 11½ft low-speed wind tunnel at the R.A.E. Farnborough during July 1968 at a nominal wind speed of 36.4 m/sec (120 ft/sec) corresponding to a Reynolds number of 0.64×10^6 based on the geometric mean chord of the wing.

3.3 Experimental results

Lift

The results plotted in Figs.29 and 30 show C_L vs wing angle of incidence, α_w, for overwing nacelles A and B respectively; the corresponding results without nacelles are also given for comparison and indicate that with internal free-flow, the nacelle effects are small over the whole incidence range tested. With the part-span flaps and leading edge droop both deflected the effect of the nacelles is similarly small with little or no influence on the values of $C_{L_{max}}$. Only when the nacelles are completely blocked internally do the results show any marked effect, i.e. a slight loss of lift near the stall, presumably when flow breakdown round the nacelle cowl, originating at the intake lip, accelerates the inboard spread of flow separations starting at the wing tips. The extreme condition of zero internal flow through both nacelles is unrealistic and is only included here to indicate the relative insensitivity of C_{L_o} to intake velocity ratio, V_t/V_o. At angles of incidence below about $10°$, C_L appears to be little affected by intake flow conditions.

The change of C_L due to nacelles, ΔC_{L_N}, is shown in Fig.31 for over-wing nacelles A and B together with the results for nacelles mounted under the wing on pylons. The results for the underslung nacelles appear to show a dependence on the flap and droop condition which is consistent with an increase of induced upwash as the droop and flap angle is increased. The lift (more strictly, normal force) on the part of the cowl forward of the wing should be expected to increase in these circumstances. The results for the overwing nacelles show a less clearly defined dependence on wing flap condition which may be due to greater interference with the flow over the upper surface of the wing. The values of ΔC_{L_N} for nacelles A and B are generally slightly higher than for the underslung nacelles below about $10°$ of wing incidence, but the differences are small.

Drag

The overall drag results for the wing and body, with and without nacelles are shown in Figs.32 to 35 as curves of C_D vs C_L^2 with flaps and droop $0°$ and with flaps $15°$ and droop $25°$. Also shown for comparison are the results for the underslung nacelles mounted on pylons, which indicate that to a first order, the lift-dependent drag (as given by the slope dC_D/dC_L^2) is close to that obtained with the wing and body alone. The corresponding value for the overwing nacelles (A and B) is about 35% higher and this trend is in broad agreement with those reported by Smelt[7] in 1939, where it was concluded that a large part of the drag increase associated with nacelles mounted unsymmetrically on the wing could be attributed to local discontinuities in the spanwise loading; whilst additional drag penalties could also be incurred from flow separations at the junctions between the nacelle and wing. The general dimensions of overwing nacelle A in the present tests do not differ, except in detailed shaping, from those described in Smelt's report. However, the requirement that the jet exit in the present tests should have a cross-section which was larger in width than height*, led to an elliptic flat shape on the top, rearward facing surface of nacelle A (hyperbolic shape for nacelle B). The clearly defined shoulders formed in this way, coupled with the marked cross-flow past the forward, cylindrical part of the cowl, caused the formation of a pair of vortices on the nacelle top surface similar to those associated with the upper surface of slender delta wings. This feature of the flow was also demonstrated in the partial model tests described earlier in the report with full-scale jet exit conditions simulated (section 2.2.4). For the complete model tests, the presence of vortices is confirmed by the surface flow patterns shown in Figs.36 and 37 for nacelles A and B respectively, using a mixture of lampblack and paraffin.

Attempts were made, on nacelle A, to modify the vortex development by fairing over the flat surface at the rear of the nacelle with plasticene, and alternatively by fitting 'end plates' at the side of the nacelle. Although the oil-flow patterns showed some alteration to the vortices, there was no significant change in the measured drag. Although it cannot be concluded from these few simple tests that it is impossible to reduce the drag associated with these nacelles, it does appear that it cannot be done easily.

---

* Ratio $W/H = 3.11$ for nacelle A and 7.15 for nacelle B.

Pitching moments

The pitching moment results with and without overwing nacelles are
presented in Figs.38 and 39 for nacelles A and B; the results for underslung
nacelles mounted on pylons are also shown for comparison. Both types of
nacelle are destabilizing as shown by the increased positive slope of the
respective C_m vs C_L curves, relative to the no-nacelle case; the destabiliz-
ing effect of each set of nacelles is approximately the same for flaps and
droop both deflected and retracted. The corresponding forward movement of
aerodynamic centre due to the underslung nacelles is about 7% of the geometric
mean chord; for overwing nacelles A and B it is about 11% and 15% respectively.
The slightly greater effect of the overwing nacelles is not thought to present
any serious longitudinal stability problem and might in practice be alleviated
when the jet is present by a redistribution of load over the wing near the
nacelles.

4   CONCLUSIONS AND RESERVATIONS

The major conclusion from these tests is presented in Figs.32 to 35,
where it is shown that the effect of adding these overwing nacelles to the
wing-fuselage model is a substantial increase in lift-dependent drag; by con-
trast, the addition of conventional pylon-mounted nacelles under the wing does
not significantly increase the lift-dependent drag above that of the wing-
fuselage model itself. All these nacelle installations were relatively crude;
in particular, no attempt was made to shape the nacelle-wing or the pylon-wing
intersections to conform to the wing flow pattern, and only limited attempts
were made to control flow separations on the nacelles themselves. Nevertheless,
the increment in lift-dependent drag is so large that it seems rather unlikely
that any simple reshaping of the nacelles would substantially improve it. If
this is accepted, it is then necessary to attempt an answer to the question
whether a similar drag penalty would be found for such an engine installation
on a full-scale aeroplane, with jets blowing over the wings. It is difficult
to give an unequivocal answer, because alternative hypotheses can be constructed
to explain the origins of the drag, and these emphasize different features of
the experimental observations.

The observed increase in drag is roughly proportional to C_L^2, which
suggests that it may be associated with a distortion of the spanwise loading.
Alternatively, the circulation defect associated with a boundary layer which
grows with increasing angle of incidence gives rise to a drag increment which

is similarly proportional to C_L^2, as pointed out for example in Ref.8, p.329. Both these effects can plausibly be associated with the strong vortices springing from the rear of the nacelle which were observed both in the low-speed tests on the complete model and in the high-speed tests with the blown jet. On this hypothesis, the fundamental cause of the large drag increment can be attributed to the load carried on the forward part of the nacelle and the associated trailing vortices shed from the rear part: effectively the nacelle acts as a small-aspect-ratio lifting surface ahead of the main wing, with a correspondingly large lift-dependent drag. Consequently, one would expect the drag results obtained with free-flow nacelles to be substantially representative of the drag of a model with the exhaust jets represented.

Two features of the experimental results are difficult to reconcile with the foregoing explanation. In the first place, it is difficult to explain why the effect should be large for the overwing nacelles but almost negligible for similar nacelles carried below the wing. The second problem is the loss of lift outboard of the nacelle in the zero-thrust condition which is illustrated in Fig.19. Vortices with the direction of rotation indicated in Figs.21 and 22 would produce an upwash on the wing at the sides of the nacelle and this should lead to an increased local lift rather than the reduction actually measured. This suggests, perhaps, that any vortices generated in the zero-thrust condition are relatively weak, and that, although such vortices were deduced from the oil-flow patterns on the complete model, they are essentially irrelevant. Following through this line of reasoning, it can be argued that the large lift-dependent drag should be associated with the 'hole' in the spanwise loading indicated in Fig.19; since this hole is effectively filled in when the jet is blown at a representative pressure ratio, the lift-dependent drag increment would, plausibly, also disappear in these circumstances.

It must be concluded that alternative interpretations can be made of the results from these tests, and it is not possible to be completely confident about the deductions to be drawn. However, it is thought that the increment in lift-dependent drag measured on the model with free-flow nacelles is likely to be found again if a test could be made with the jets simulated, and that this is likely to be true also for a full-scale aircraft of this configuration. To confirm this conclusion would require tests with a much more elaborate model, probably with some form of blown or powered nacelles.

Although the result of these tests can fairly be described as disappointing it is important to remember that the drag penalty is only one aspect of this type of engine installation, and it could be balanced by other advantageous features of the layout. For example, the saving in undercarriage weight can be set against the increased fuel weight needed to maintain the range of the aircraft with the higher drag of the over-wing installation. Only detailed 'trade-off' studies by the designer can determine which installation is best for a given aircraft and engine specification. As engine bypass ratio is increased, the problem of providing ground clearance increases; at the same time, the thrust available for take-off is increasingly greater than the cruise thrust. The table below gives the results of some simple calculations by Kirkpatrick for a twin-engined short-range transport intended to cruise at M_o = 0.8 at 30000 feet. We compare three cases: the datum aircraft has an effective aspect ratio* of 7 and engines of bypass ratio 5:1 which are sized to meet the airworthiness requirement of a minimum climb gradient of 0.024 with one engine failed. If the engine bypass ratio is increased to 8:1 while the cruise thrust is kept constant, the take-off distance is reduced by 13% and the climb gradient increased to 0.037. If it is assumed that fitting these larger engines in an over-wing position reduces the effective aspect ratio to 5, the cruise thrust must be increased by 10% to maintain the cruising speed. With these engines, the take-off distance is still 10% less than for the datum aircraft, and the single-engined climb requirement is still met. Thus even an increase of 40% in lift-dependent drag is perhaps tolerable, if the other advantages of the layout can be realised.

Aircraft	A	B	C
Engine bypass ratio	5:1	8:1	8:1
Effective aspect ratio*	7	7	5
Thrust/weight ratio:			
At cruise	0.070	0.070	0.077
At take-off	0.220	0.246	0.271
Single-engined climb gradient	0.024	0.037	0.024
Single-engined take-off distance	2395 m	2092 m	2154 m

---

* Effective aspect ratio is defined as A/K, where A is the geometric aspect ratio and K the lift-dependent drag factor defined by $C_{D_i} = K\, C_L^2/\pi A$.

SYMBOLS

c	wing chord
C_D	drag coefficient
ΔC_D	C_D with thrust $-$ C_D at zero thrust
C_L	lift coefficient
ΔC_L	C_L with nozzle (or nacelles) present $-$ C_L wing alone
C_m	pitching-moment coefficient; axis through the mean $\frac{1}{4}$ chord point of the wing
C_p	pressure coefficient
C_p^*	critical pressure coefficient (for which $M = 1$ locally)
$C_{T_{net}}$	net thrust coefficient
H	local stagnation pressure
ΔH	$H - H_o$
H_j	stagnation pressure of jet stream at nozzle exit
H_o	stagnation pressure of free stream
M_o	free stream nominal Mach number
p	local static pressure
$\bar{p}_j$	mean static pressure acting on the upper surface of the wing behind the nozzle
p_o	static pressure in free stream
R_n	radius of nozzle
V_o	velocity of free stream
V_t	velocity of flow at nacelle throat
x	distance along wing chord from the leading edge
y	spanwise distance along wing from the nozzle centre-line
α_w	angle of incidence of wing

REFERENCES

No.	Author(s)	Title, etc.
1	H. C. Garner	Subsonic wind tunnel wall corrections. Chapter 6: wall interference in tunnels with ventilated walls. Agardograph 109 (1966)
2	A. G. Kurn	A suction control system for the boundary layer developed along a cylinder. Unpublished MAS material (1968)
3	R. A. Pinker H. V. Herbert	Tests of a rectangular asymmetric ramp nozzle in quiescent air. N.G.T.E. Note NT 620 (1966)
4	A. G. Kurn	A further wind tunnel investigation of underwing jet interference. ARC CP 1156 (1969)
5	D. J. Kettle	R.A.E. Report to be published
6	J. A. Bagley D. J. Kettle	Brief tests on a faired nacelle. R.A.E. unpublished work
7	R. Smelt	The installation of an engine nacelle on a wing. ARC R. & M. 2406 (1939)
8	B. Thwaites	Incompressible aerodynamics. Oxford University Press (1960)
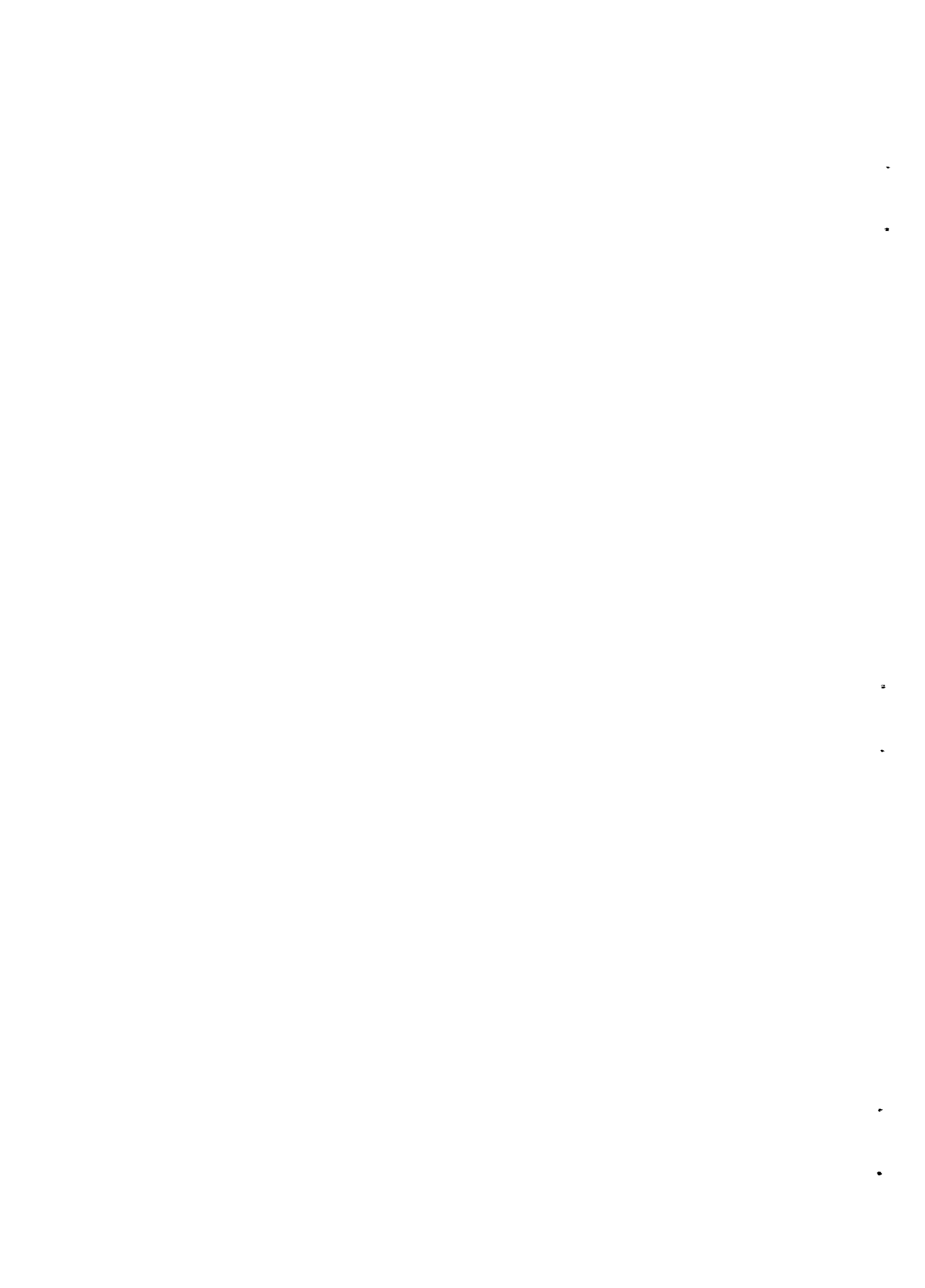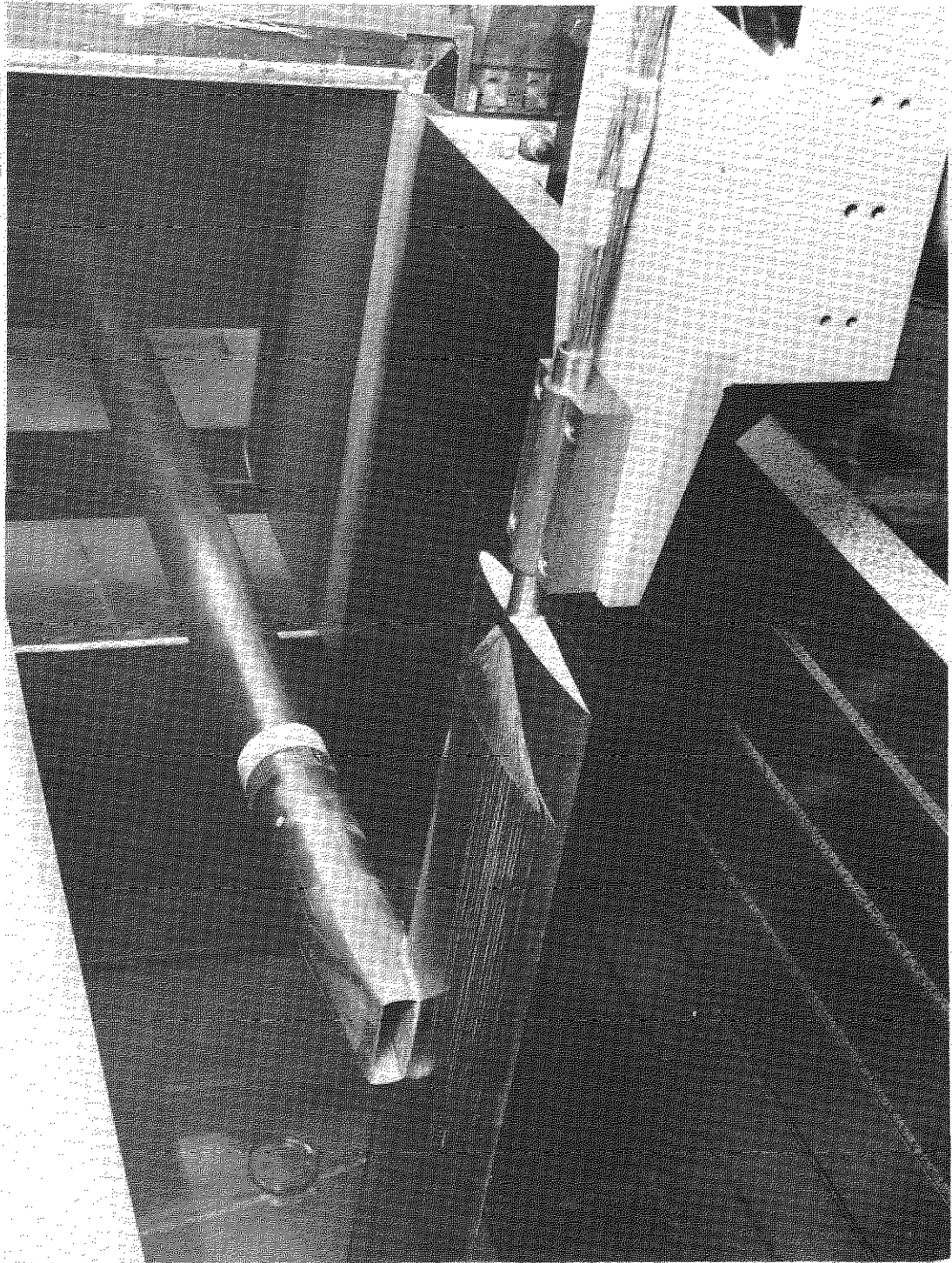
Fig.1. Test rig
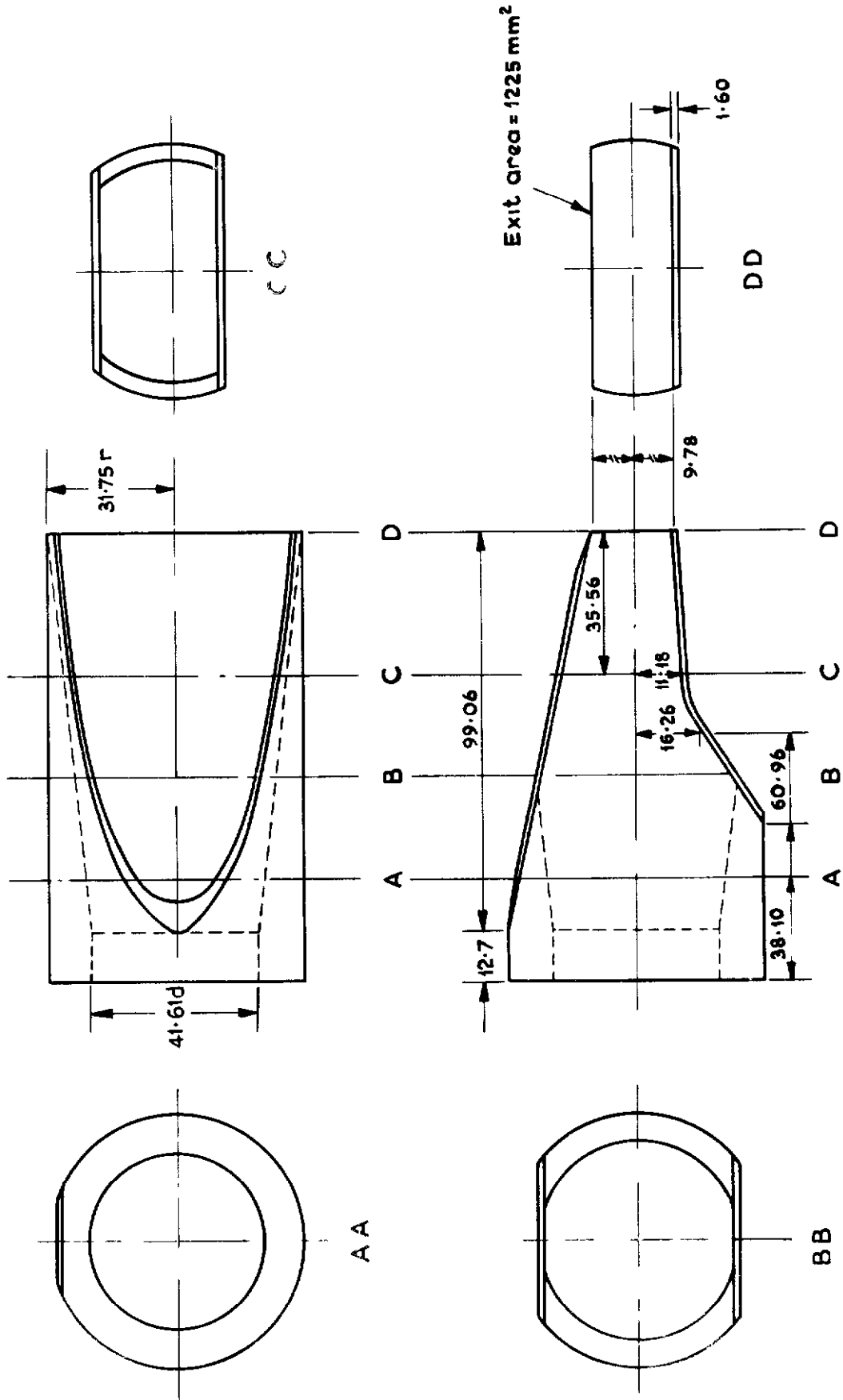
Fig.2 Nozzle

Dimensions in millimetres

Exit area = 1225 mm²

0.315 c

R_n

31.75 mm

y

$y/R_n = 0$ 1 36   2·60

1 80

Chordwise static hole positions
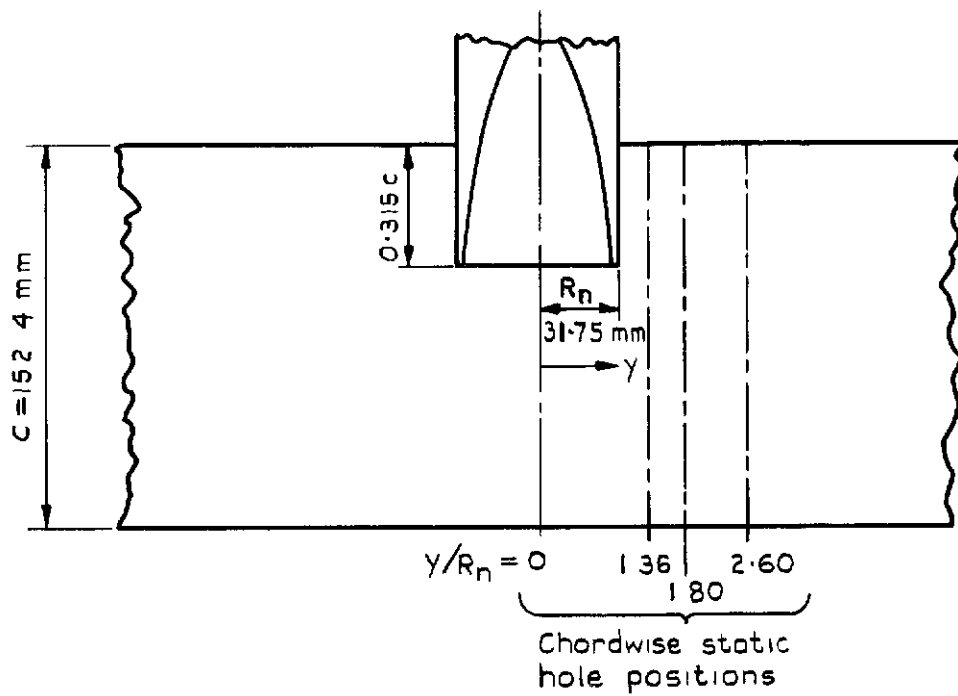
M_0	H_j/P_0	H_j/H_0	$C_{\tau \, net}$	y/R_n
0·60	1·276	1·00	0	0, 1 36, 1·80, 2·60
	2·40	1·88	3·64	0, 1·36, 1·80, 2·60
0·66	1 340	1 00	0	0
	2 40	1 79	2·66	0
0 70	1·387	1·00	0	0
	2·40	1 73	2·18	0
0 72	1·412	1 00	0	0
	2·40	1 70	1 97	0
0 74	1 439	1 00	0	0, 1·36, 1·80, 2 60
	1 73	1 20	0 53	0
	2·01	1 40	1·05	0
	2 21	1 54	1 41	0
	2·31	1 61	1 58	0
	2·40	1 67	1 77	0, 1 36, 1·80, 2 60
	2 54	1 77	2 12	0
	2 98	2·07	2 88	0

Fig. 3 Wing-nozzle configuration and test programme
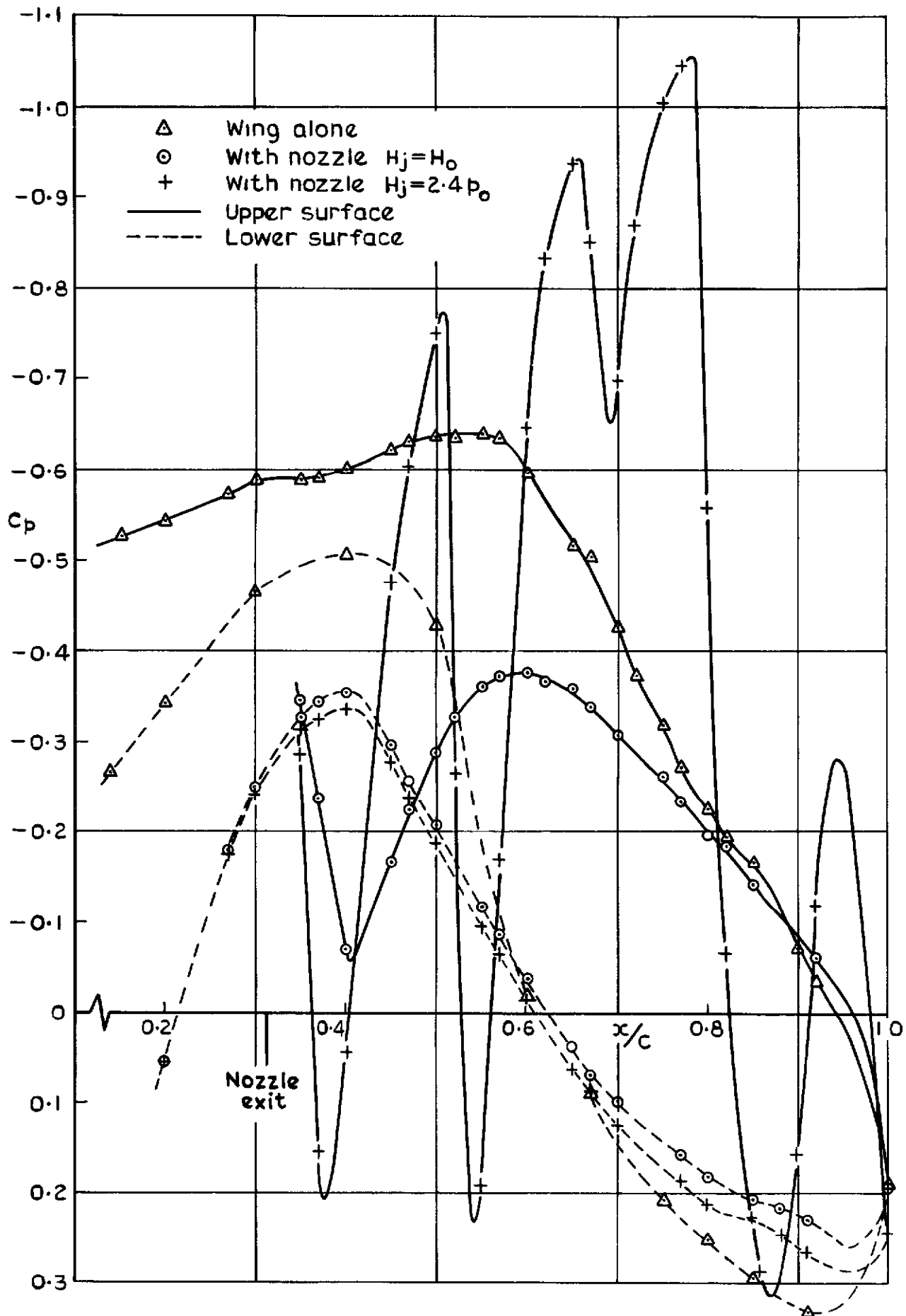
Fig. 4 Effect on wing pressures at $y/R_n = 0$ due to the presence
of the nozzle with and without jet thrust. $M_o = 0.74$
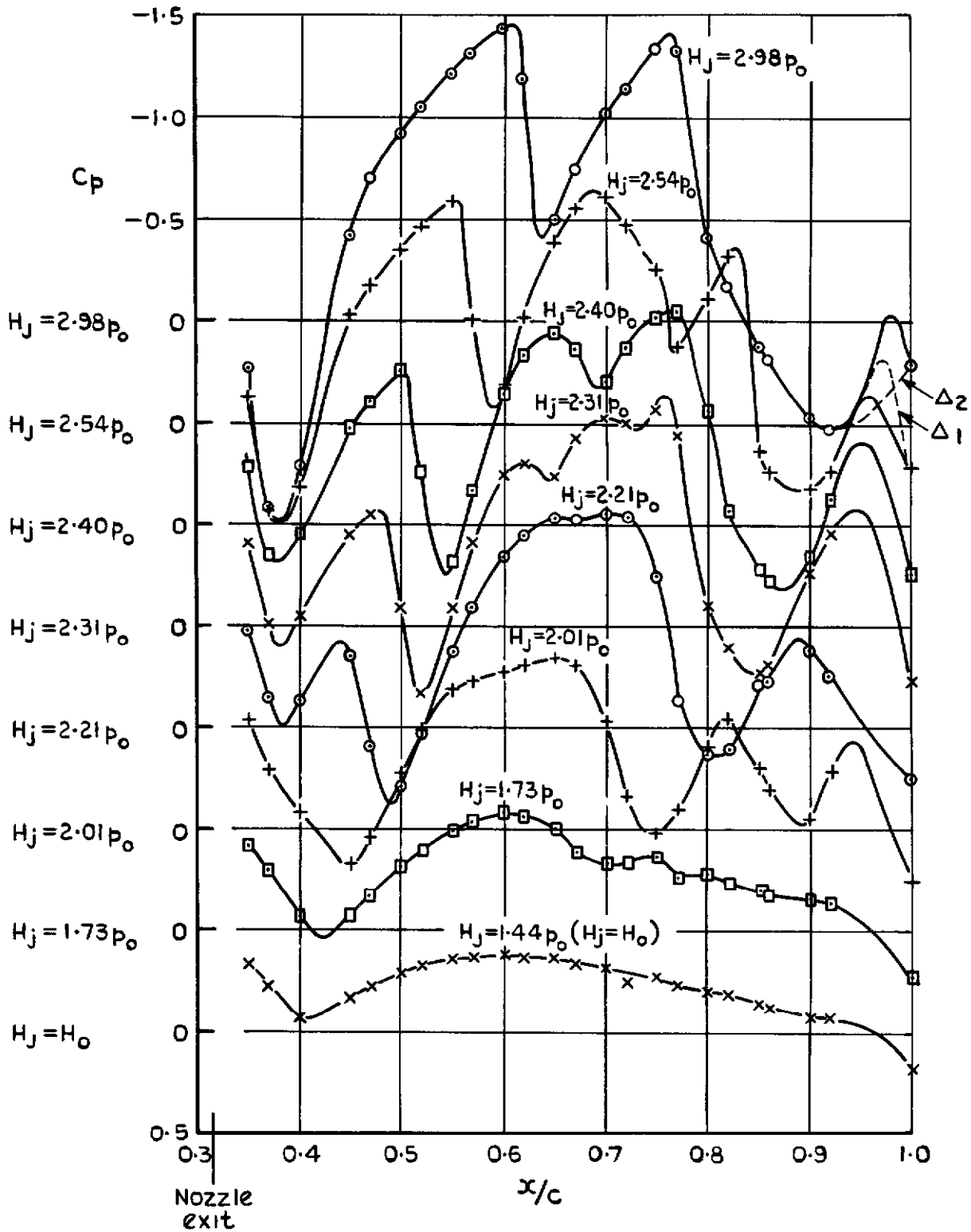
Fig. 5 Effect of varying jet flow on the wing
upper surface at $y/R_n = 0$. $M_o = 0.74$

$H_j = 2.98\ p_0$

$H_j = 2.54\ p_0$

$H_j = 2.40\ p_0$

$H_j = 2.31\ p_0$

$H_j = 2.21\ p_0$

$H_j = 2.01\ p_0$

$H_j = 1.73\ p_0$

$H_j = H_0$
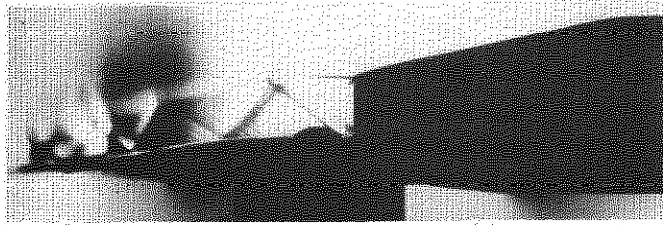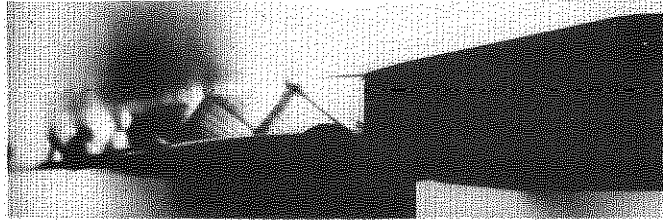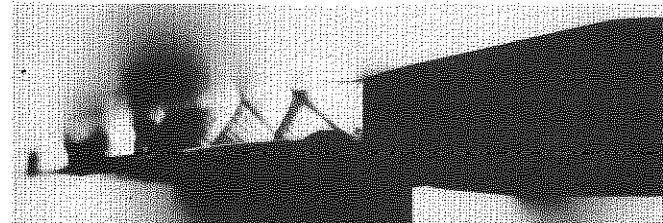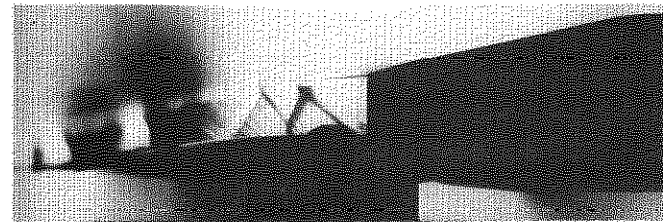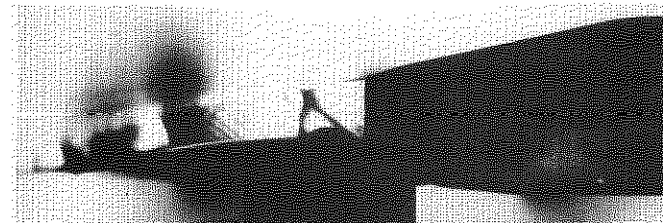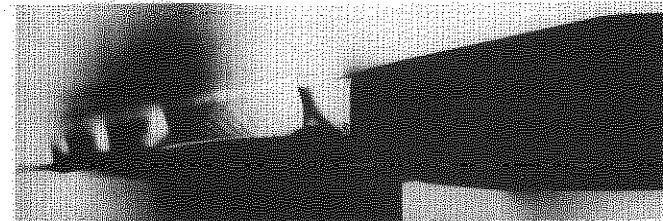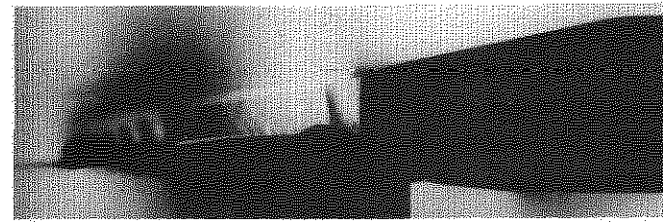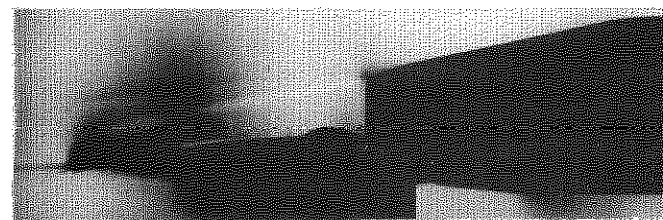
Fig.6. Schlieren photographs at varying jet flow conditions. $M_0 = 0.74$
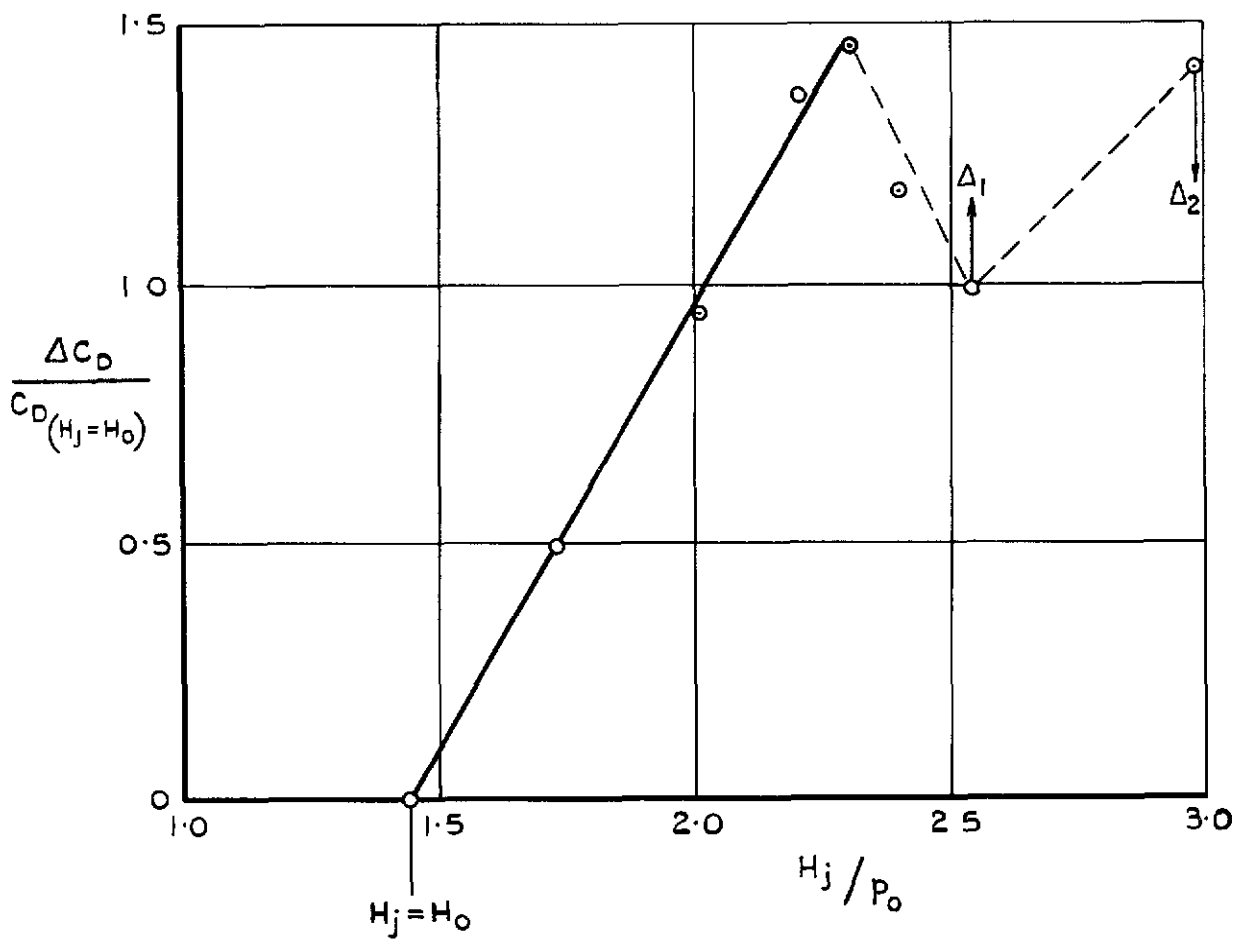
Fig.7 Variation of drag with jet flow on the part of the wing
behind the nozzle (upper surface, 0·35c to 1·00c)
$y/R_n = 0$ $M_o = 0·74$
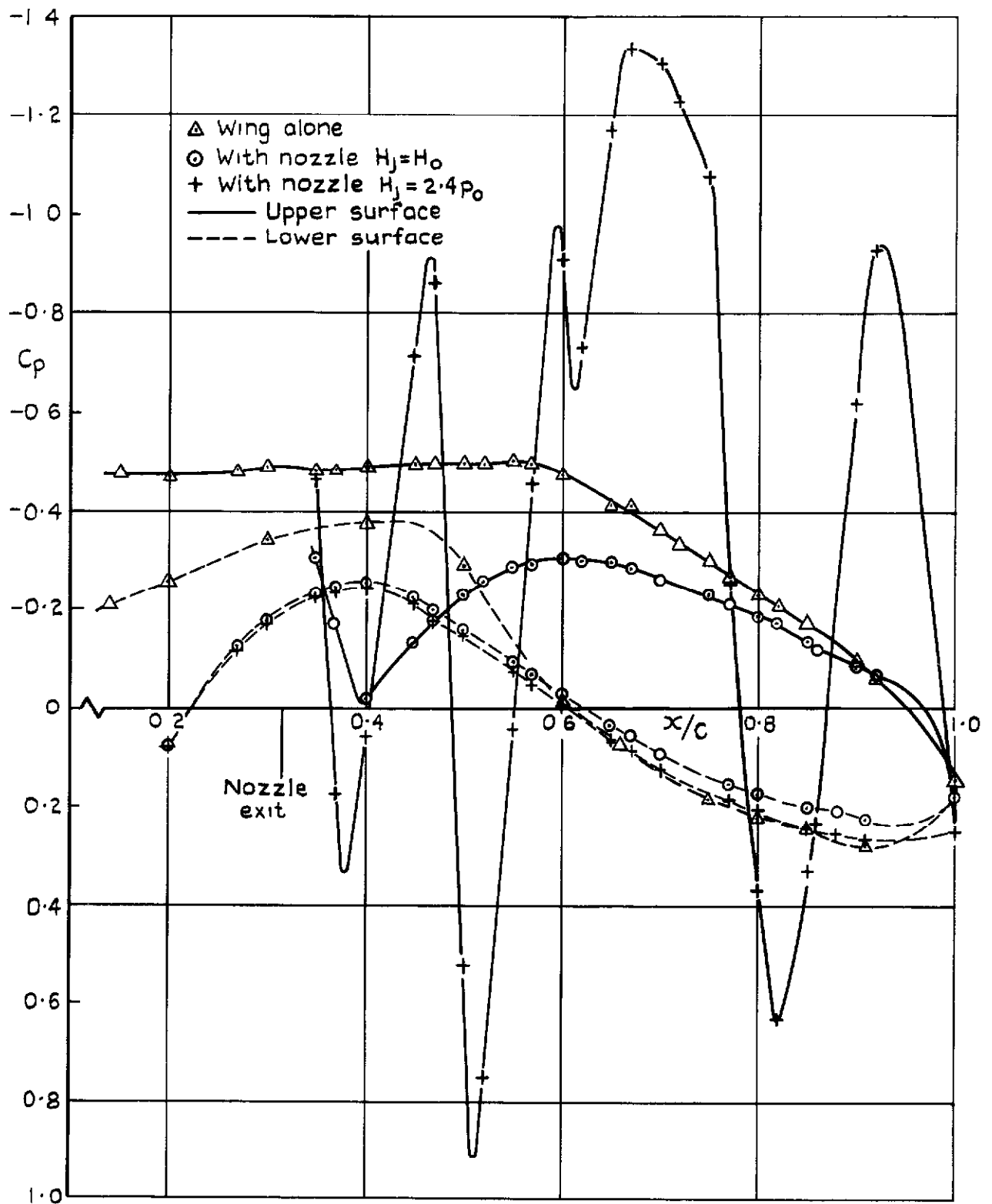
Fig. 8 Effect on wing pressures at $y/R_n = 0$ due to the presence of the nozzle with and without jet thrust. $M_o = 0.60$
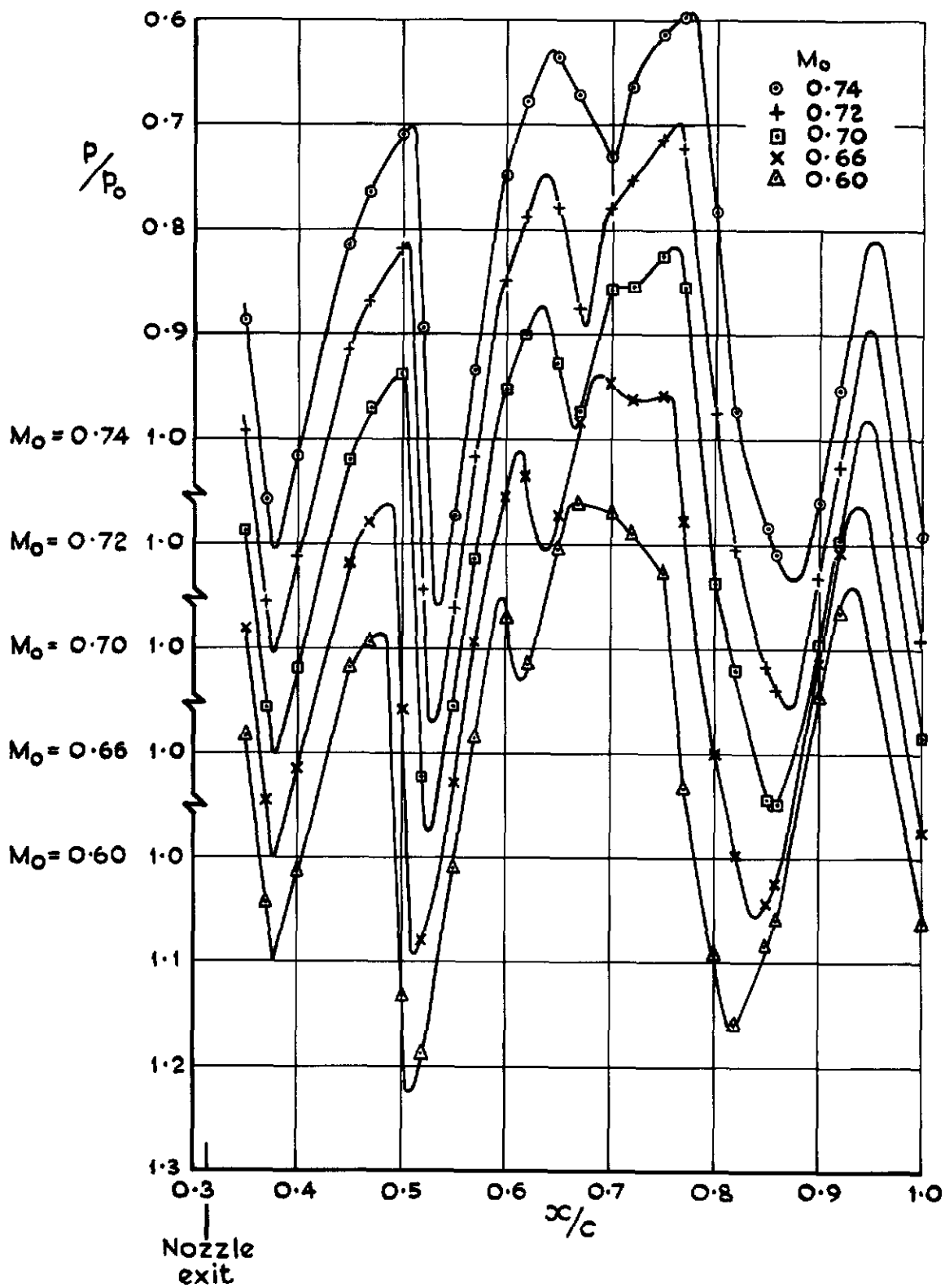
Fig.9 Effect of free stream Mach number on the wing upper–surface at $y/R_n = 0$, with $H_j/p_o = 2\cdot4$
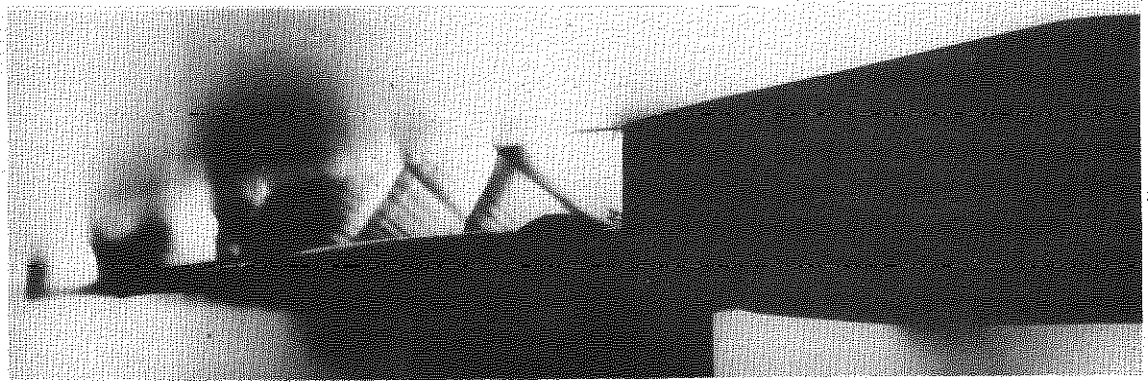
$M_0 = 0.74$
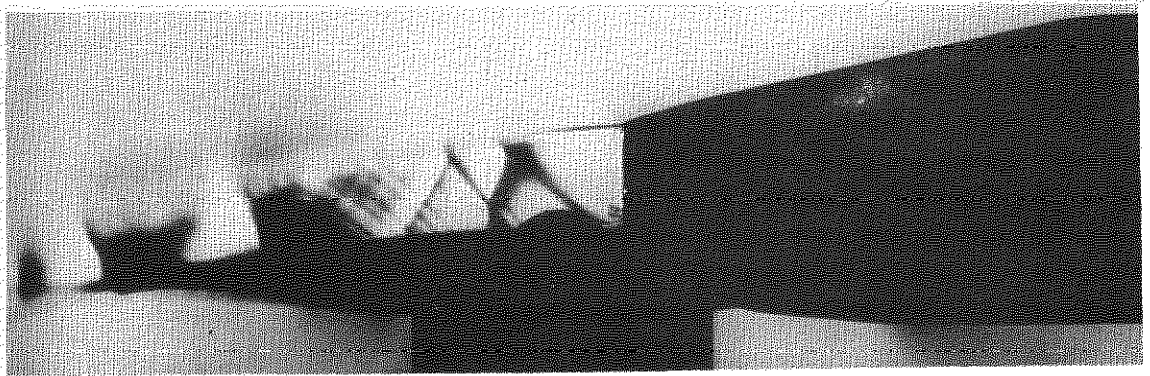
$M_0 = 0.60$

Fig.10. Schlieren photographs at two Mach numbers. $H_j/p_0 = 2.4$
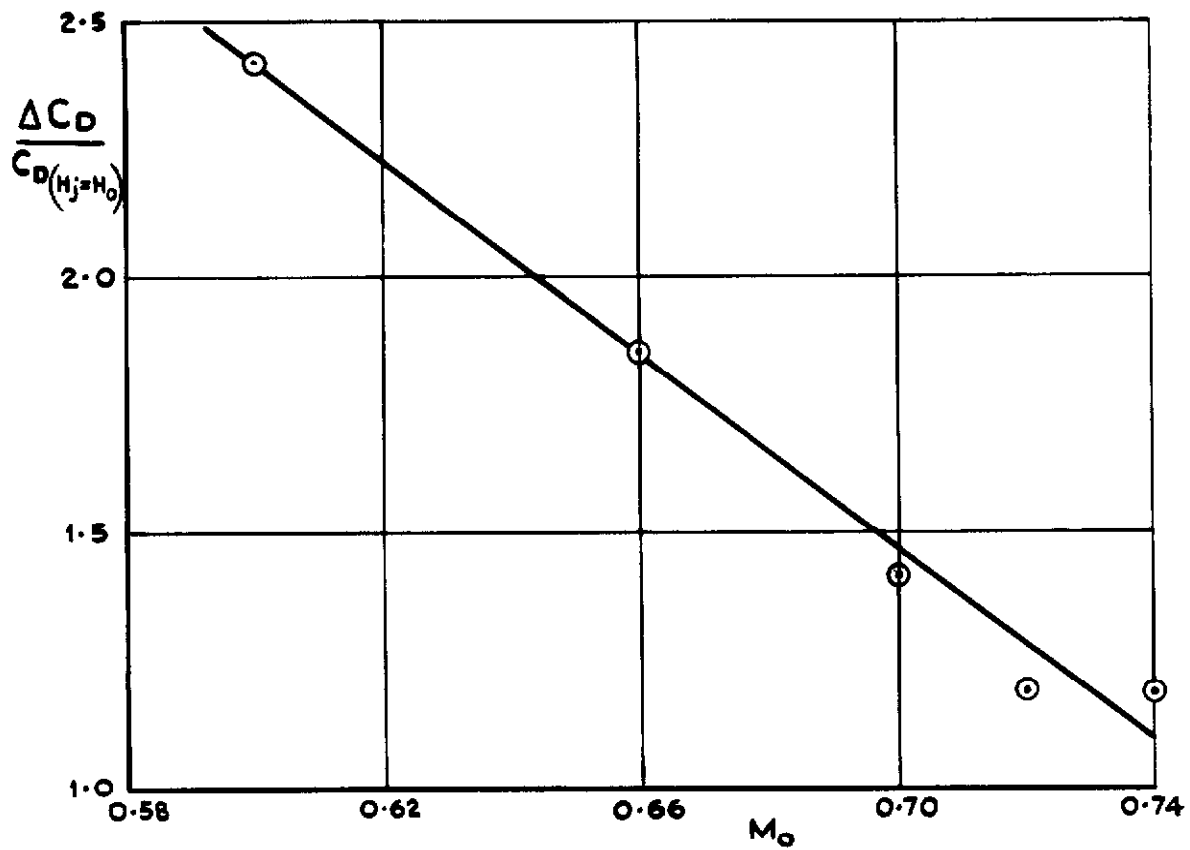
Fig.11 Variation of drag with Mach number on the part of the wing behind the nozzle $(0.35c-1.0c)$. $y/R_n=0.$ $^{H_j}/_{P_0}=2.4$
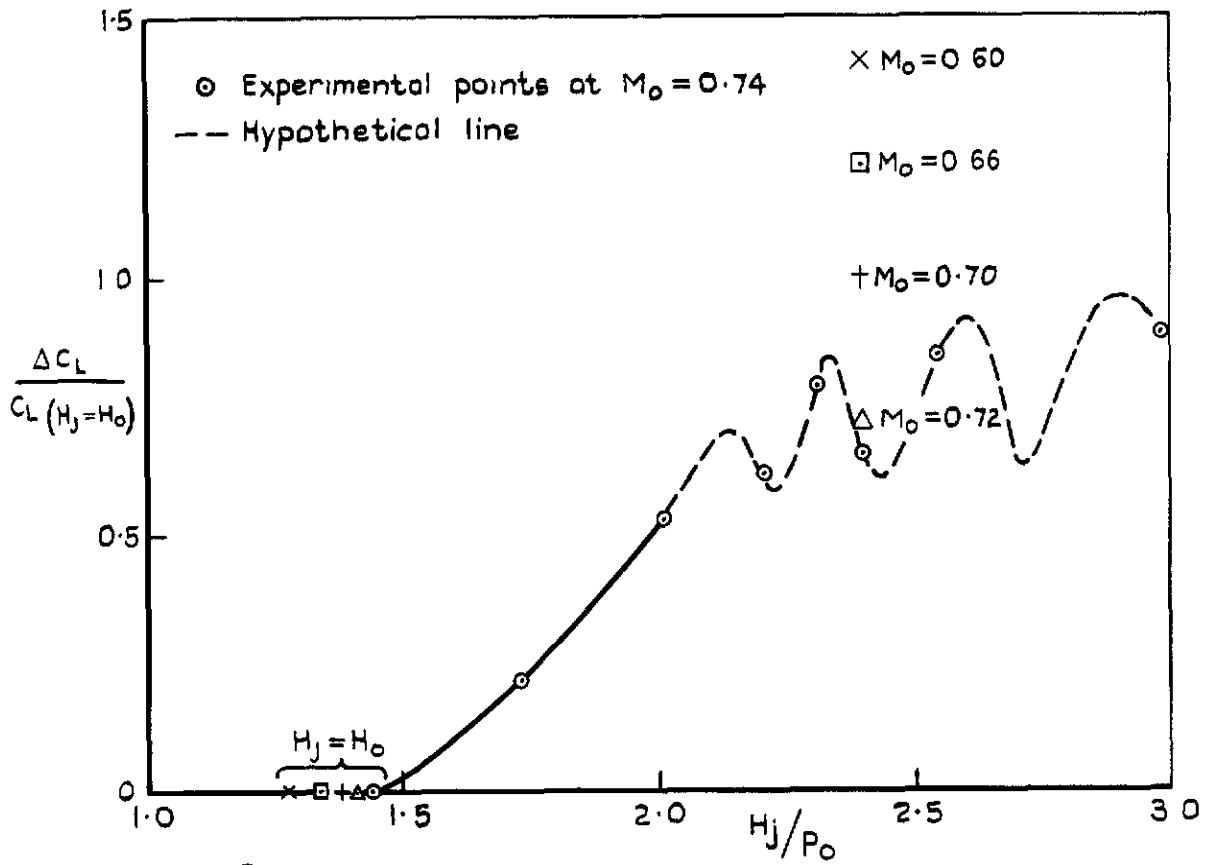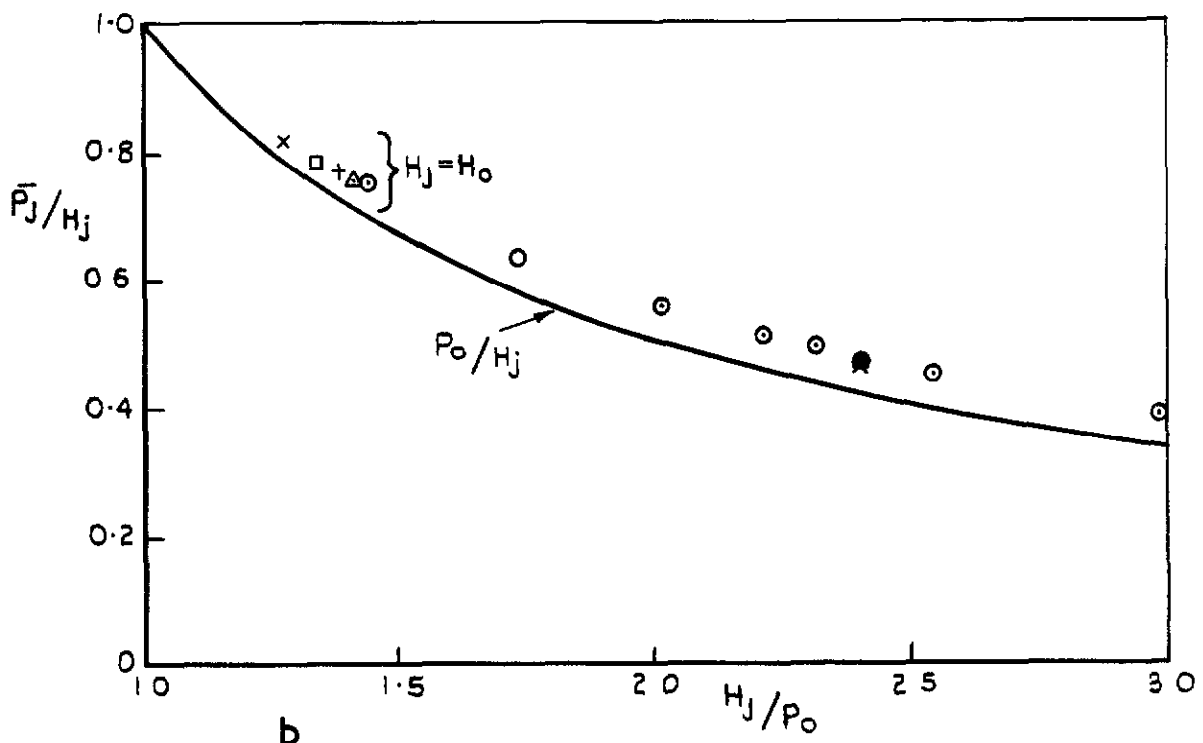
Fig. 12a&b Variation of lift on the part of the wing
behind the nozzle $(0.35c - 1.00c)$ $y/R_n = 0$
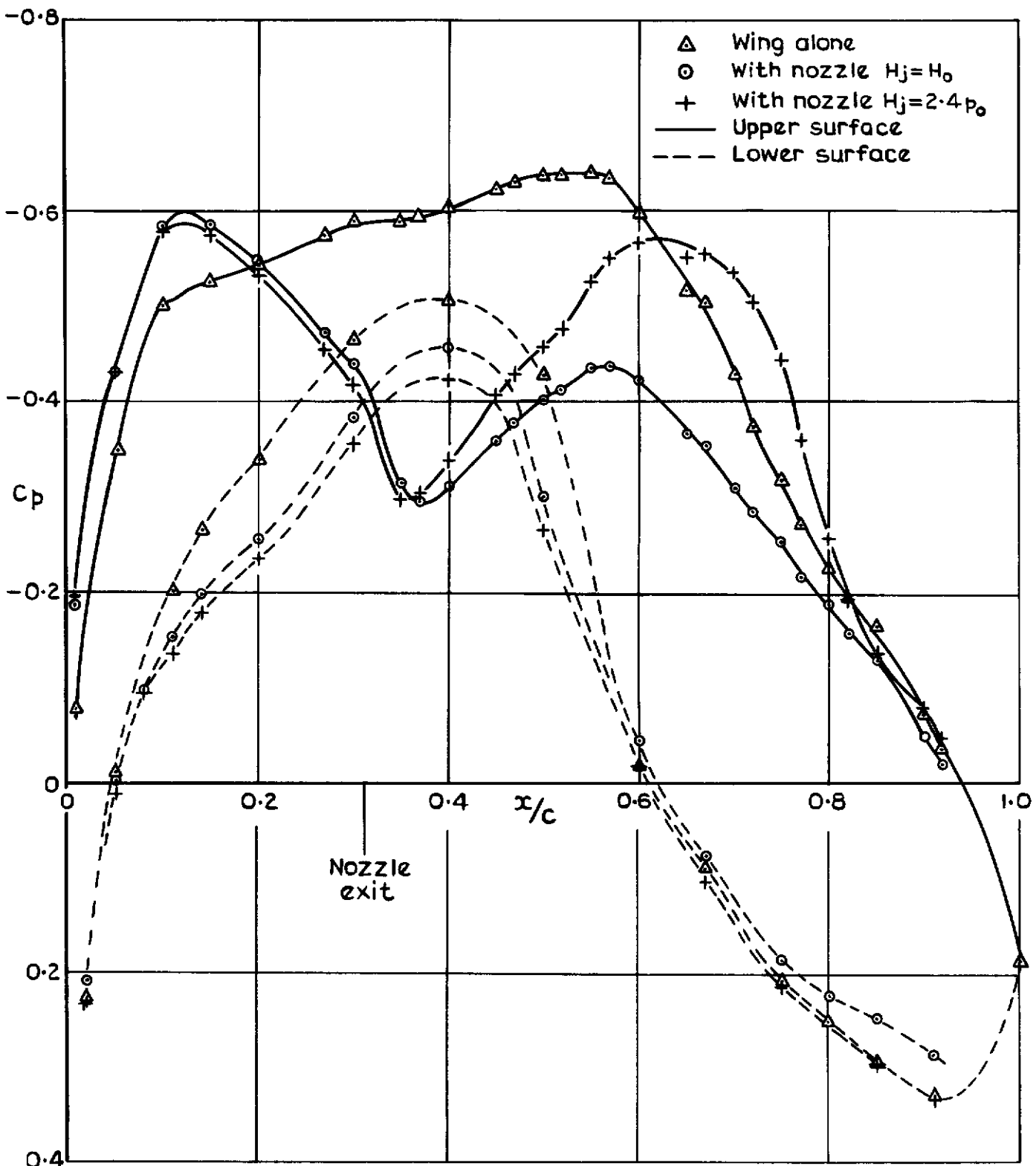
Fig. 13 Effect on wing pressures at $y/R_n = 1.36$ due to the presence of the nozzle with and without jet thrust. $M_o = 0.74$
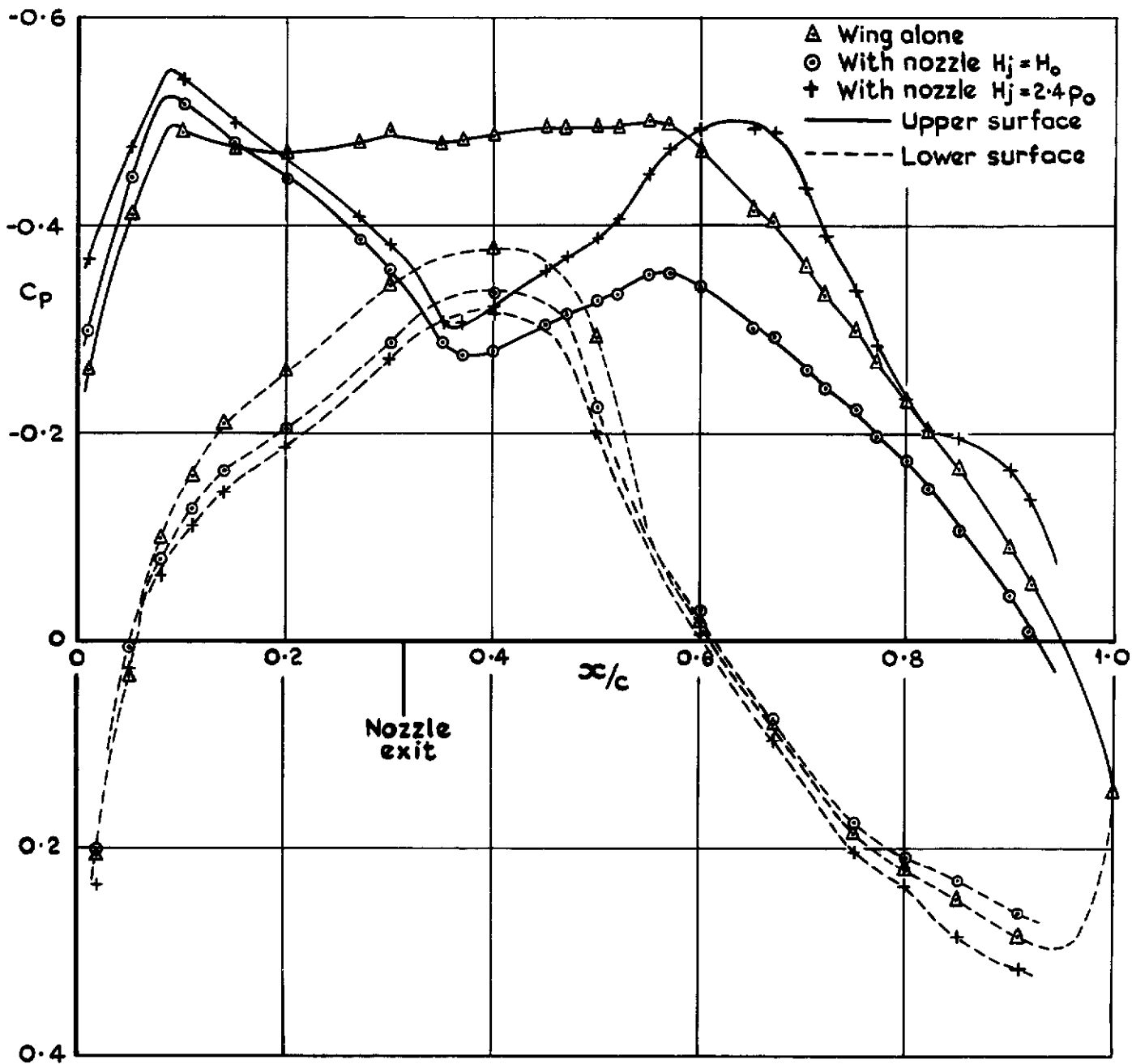
Fig.14 Effect on wing pressures at $y/R_n = 1.36$ due to the presence of the nozzle with and without jet thrust. $M_o = 0.60$
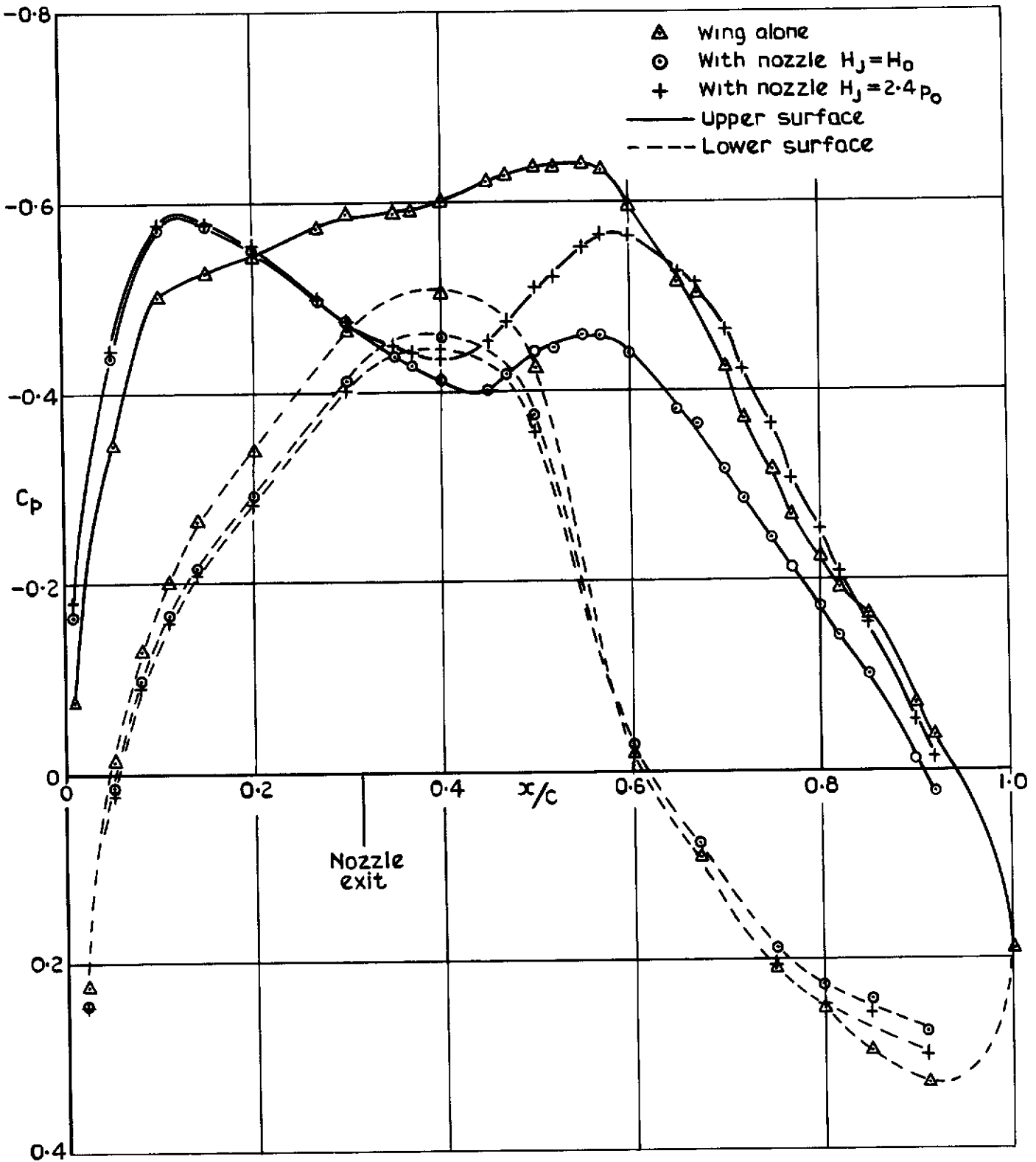
Fig. 15 Effect on wing pressures at $y/R_n = 1 \cdot 80$ due to the presence
of the nozzle with and without jet thrust. $M_0 = 0 \cdot 74$
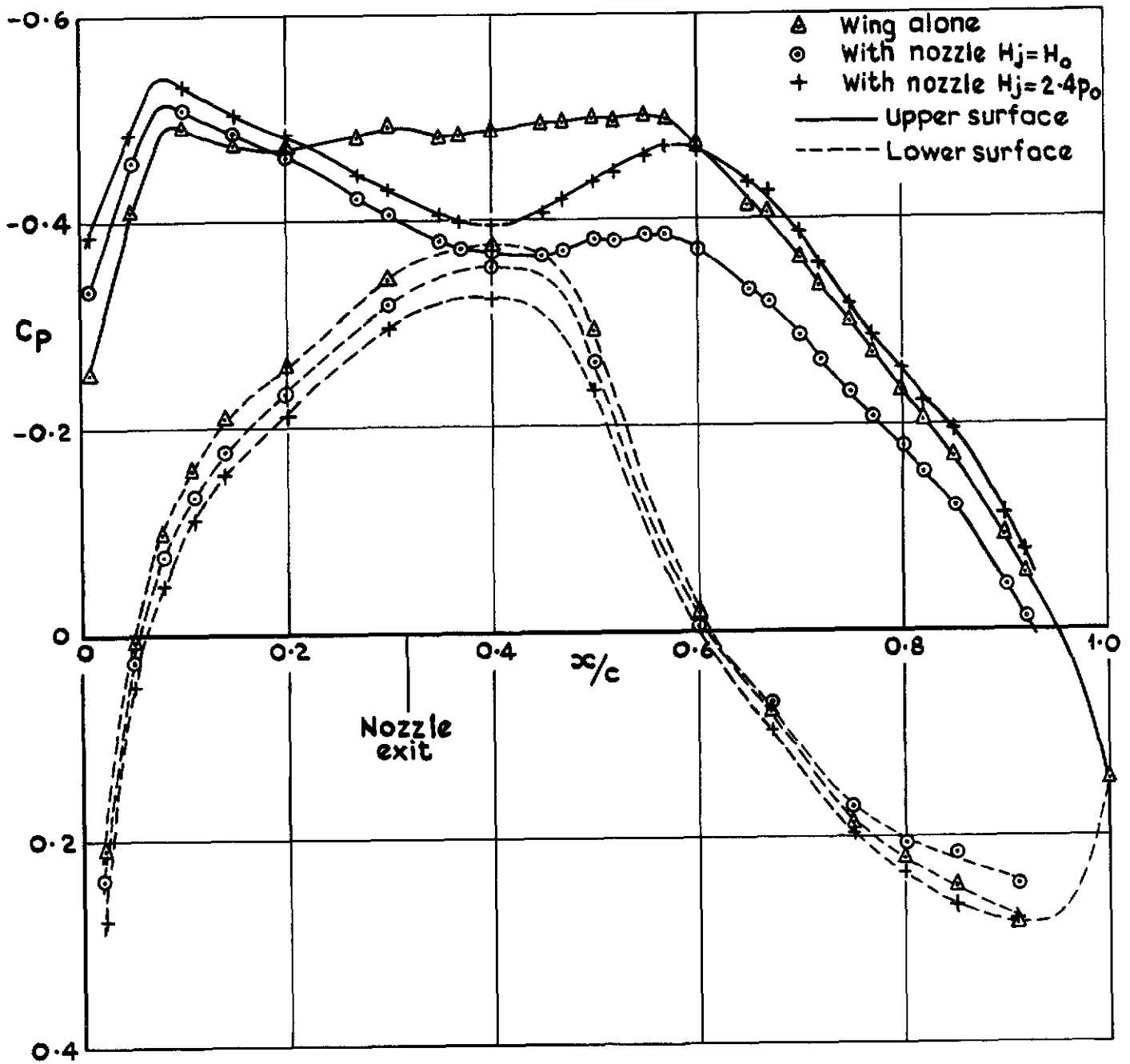
Fig.16 Effect on wing pressures at $y/R_n = 1.80$ due to the presence of the nozzle with and without jet thrust. $M_o = 0.60$
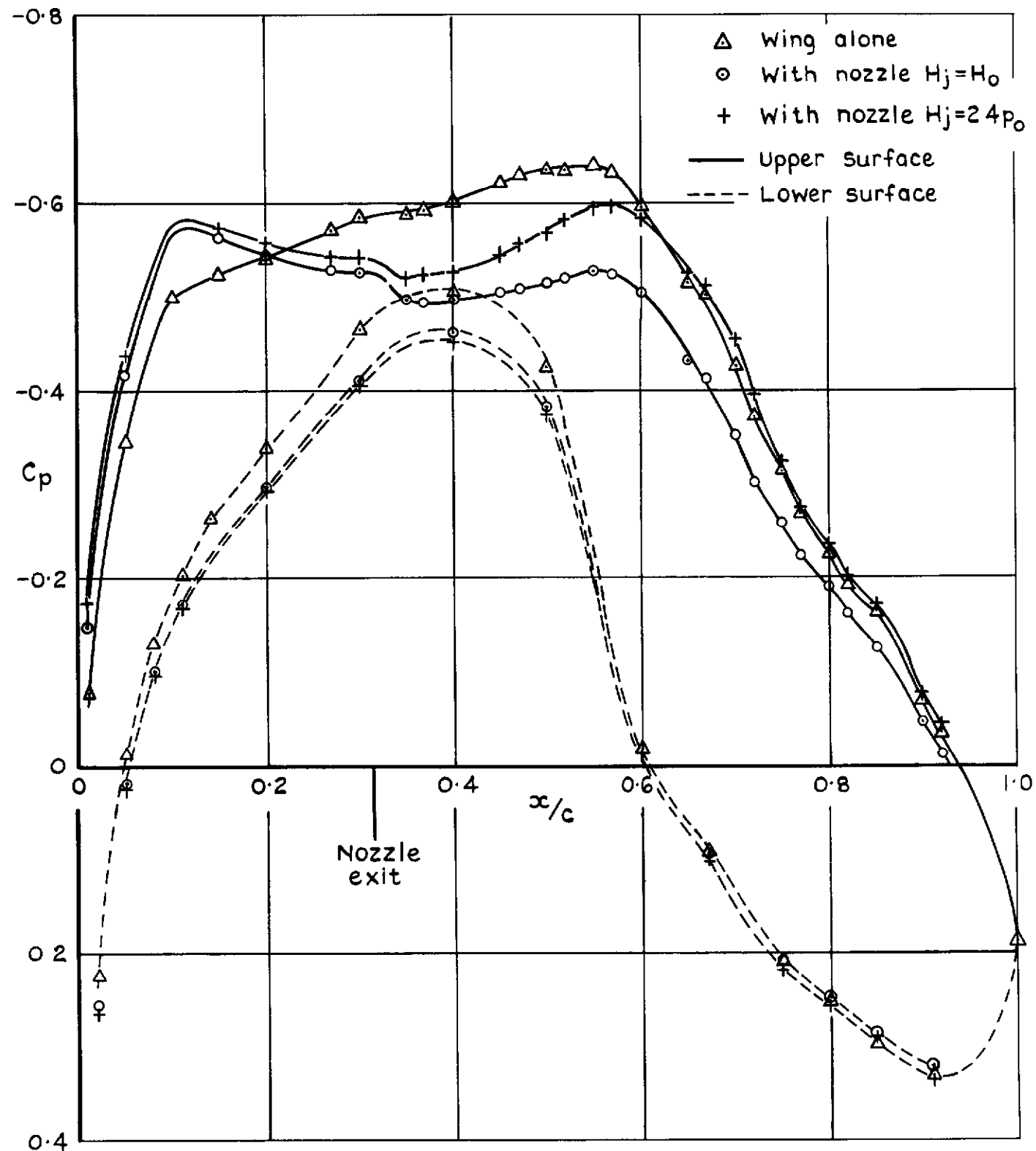
Fig.17 Effect on wing pressures at $y/R_n = 2.60$ due to the presence of the nozzle with and without jet thrust. $M_0 = 0.74$
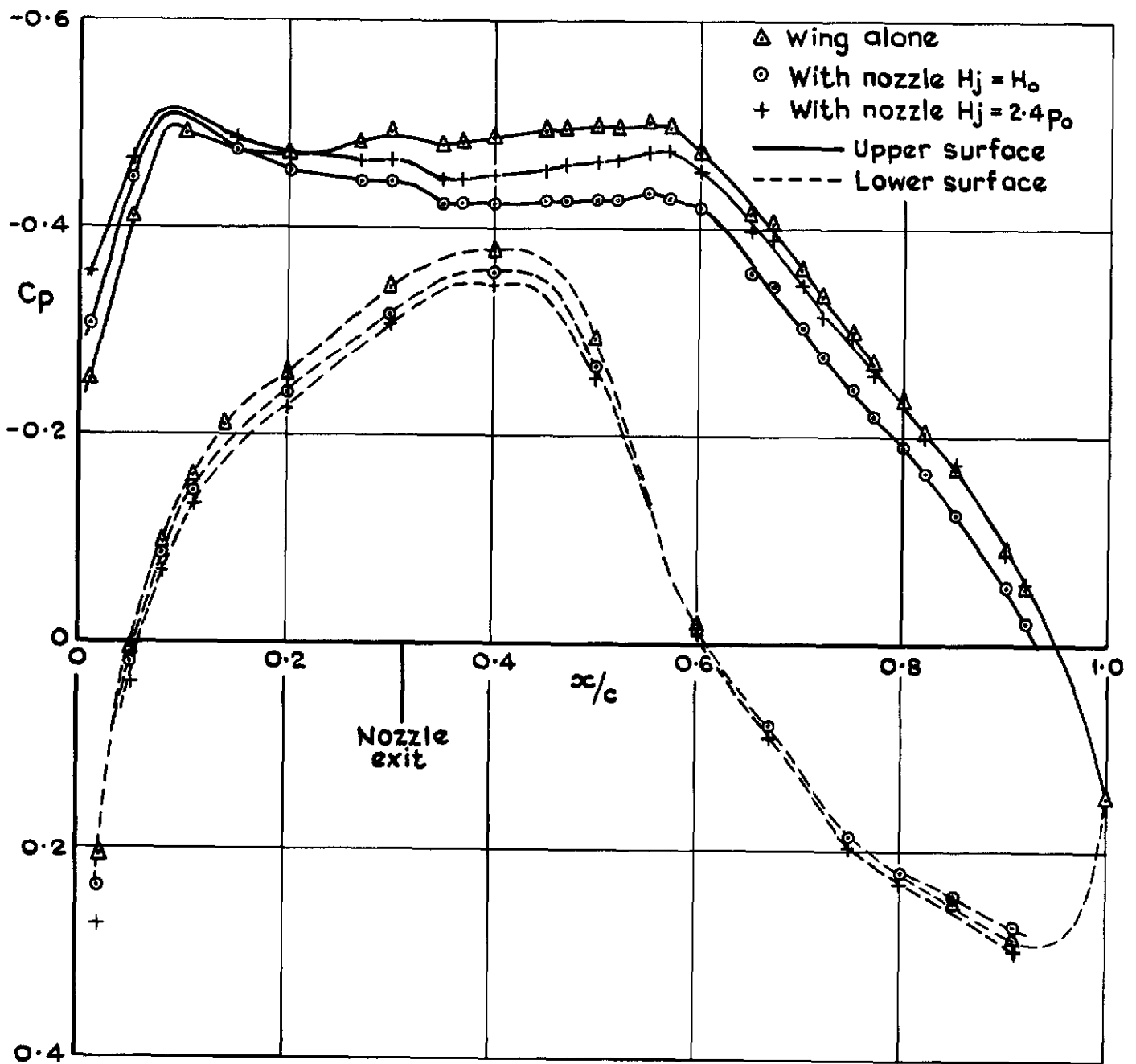
Fig.18 Effect on wing pressures at $y/R_n = 2.60$ due to the presence of the nozzle with and without jet thrust $M_o = 0.60$
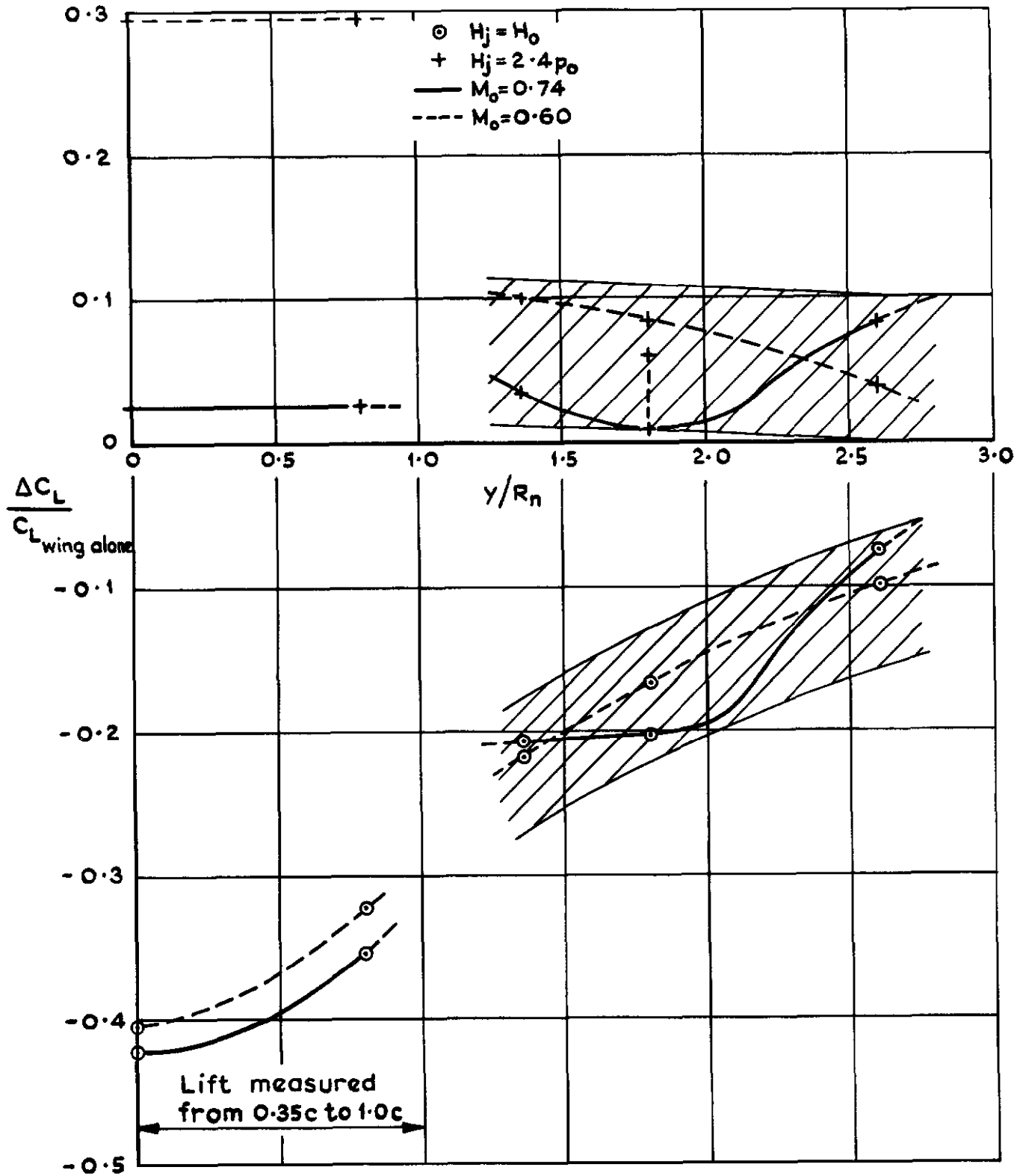
Fig.19 The effect on wing lift due to the presence
of the nozzle with and without jet thrust
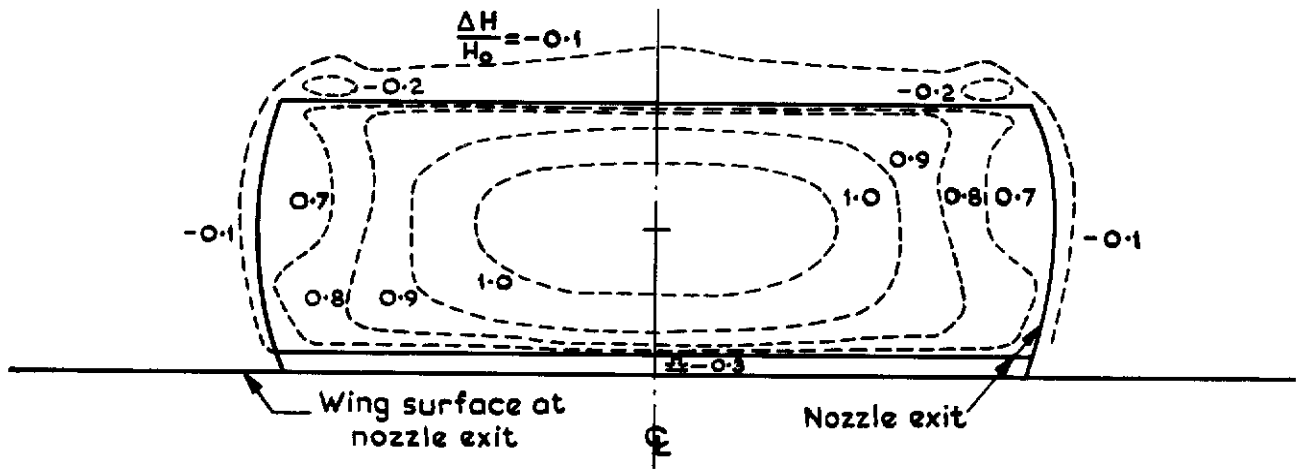
$$a \qquad M_o = 0 \cdot 60 : \ ^{Hj}/_{H_o} = 1 \cdot 88$$
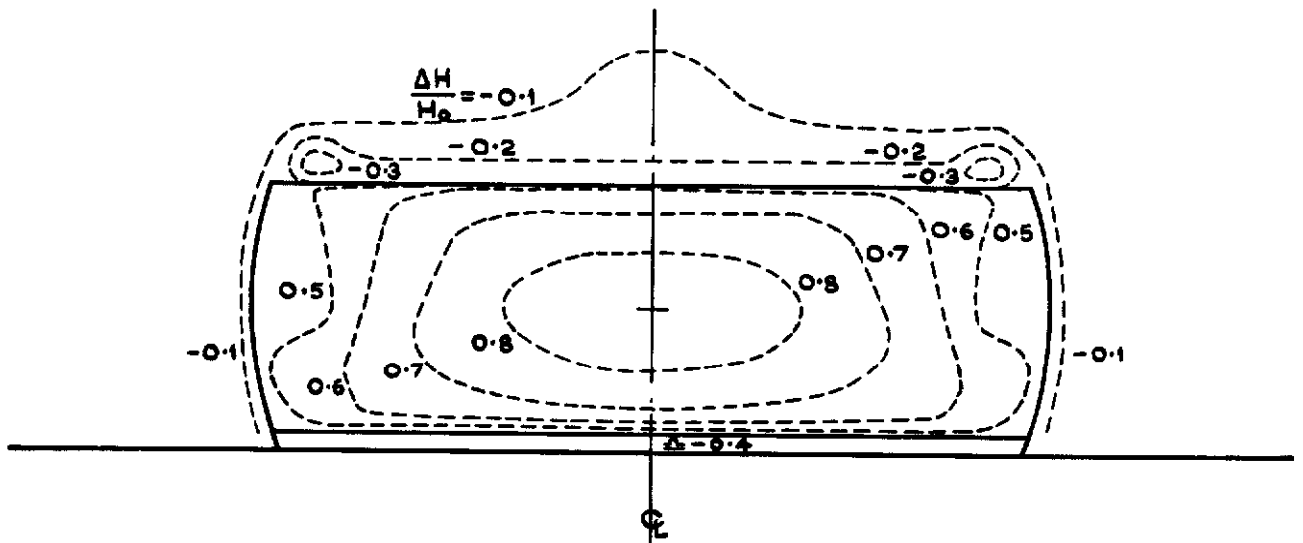
$$b \qquad M_o = 0 \cdot 74 : \ ^{Hj}/_{H_o} = 1 \cdot 67$$

Fig.20 a & b Total pressure distribution at nozzle exit
with $^{Hj}/_{P_o} = 2 \cdot 4$
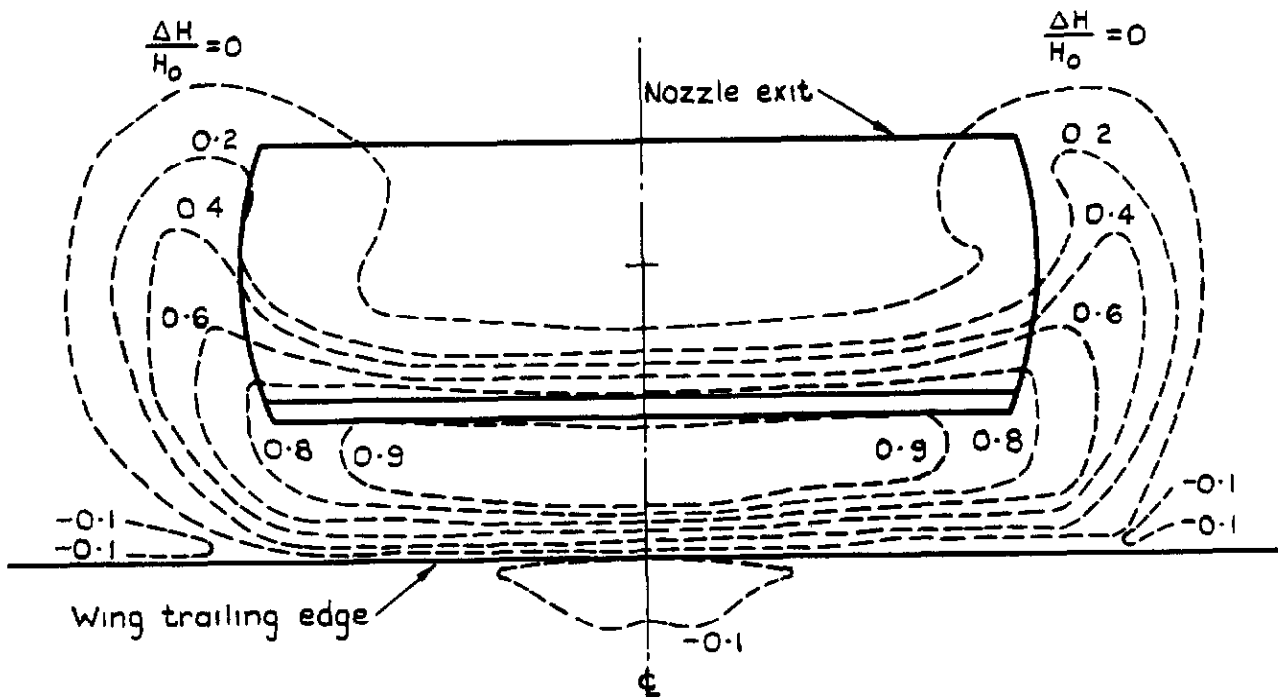
a $M_o = 0.60$: $H_j/H_o = 1.88$
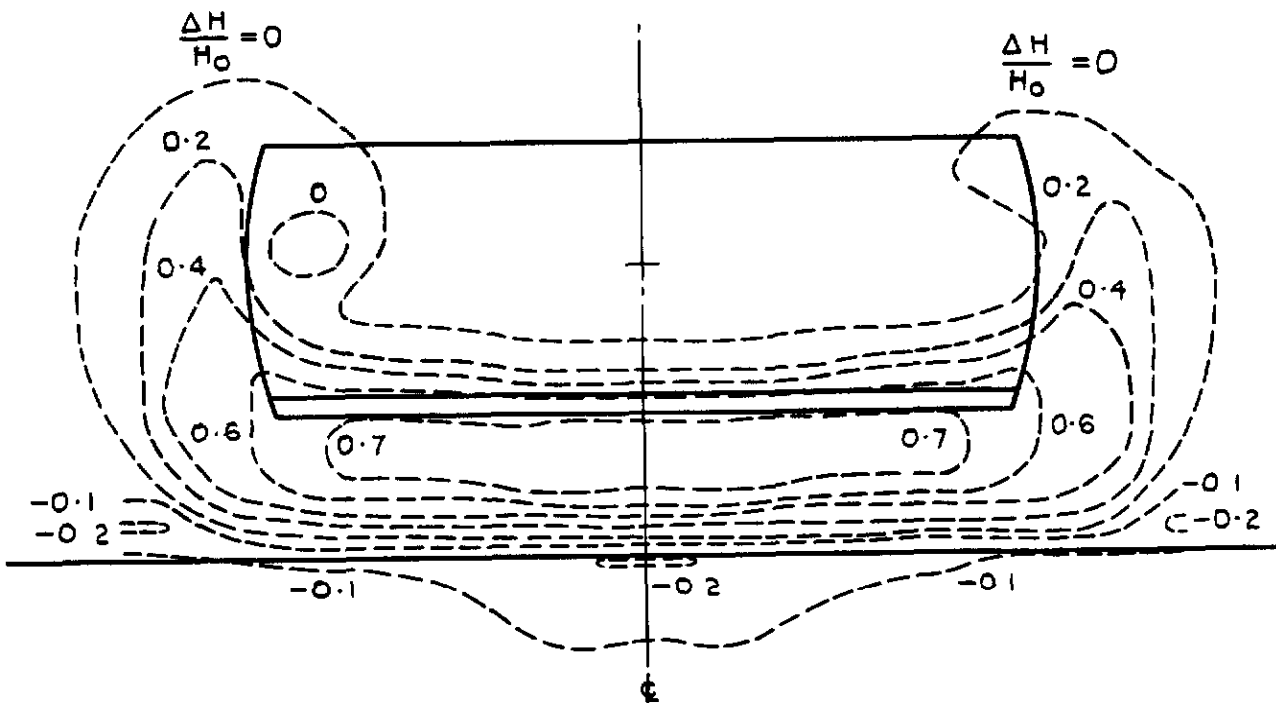
b $M_o = 0.74$: $H_j/H_o = 1.67$

Fig. 21 a & b Total pressure distribution at wing trailing edge with $H_j/p_o = 2.4$
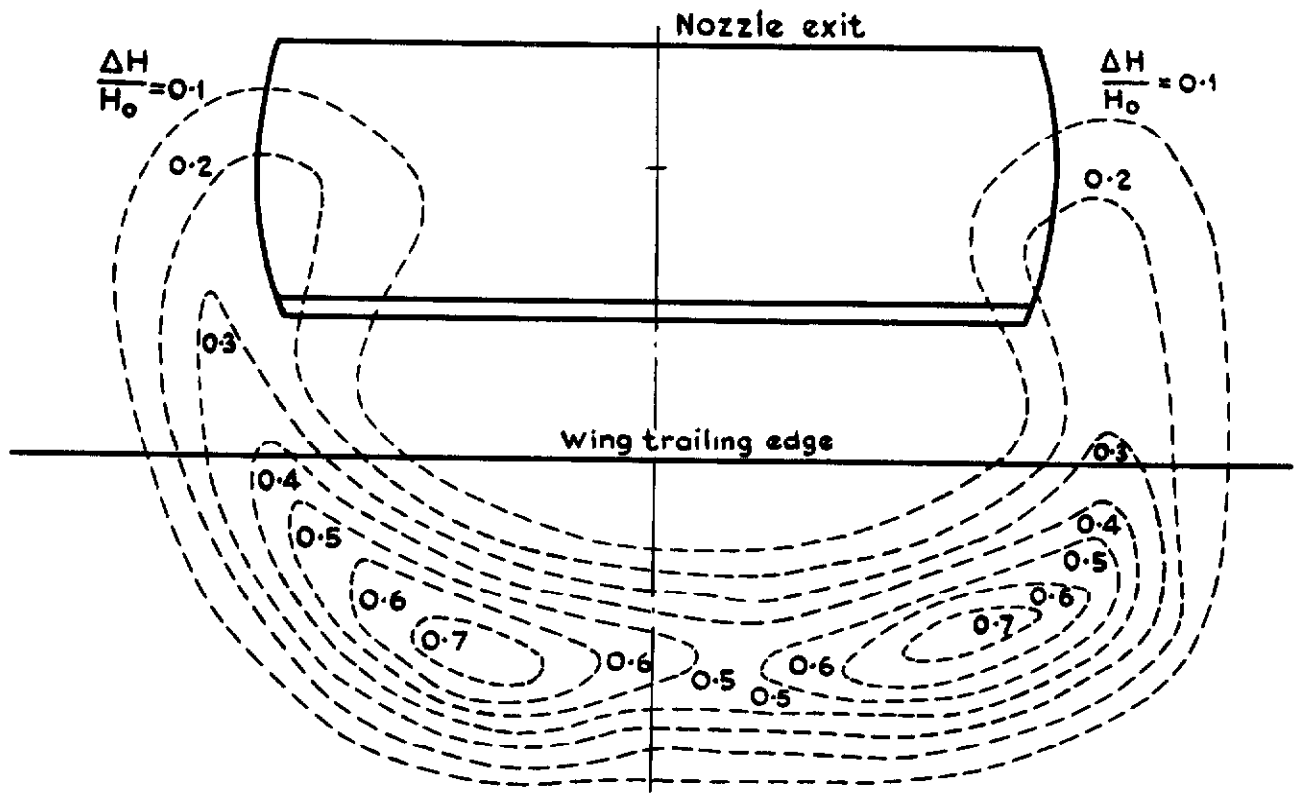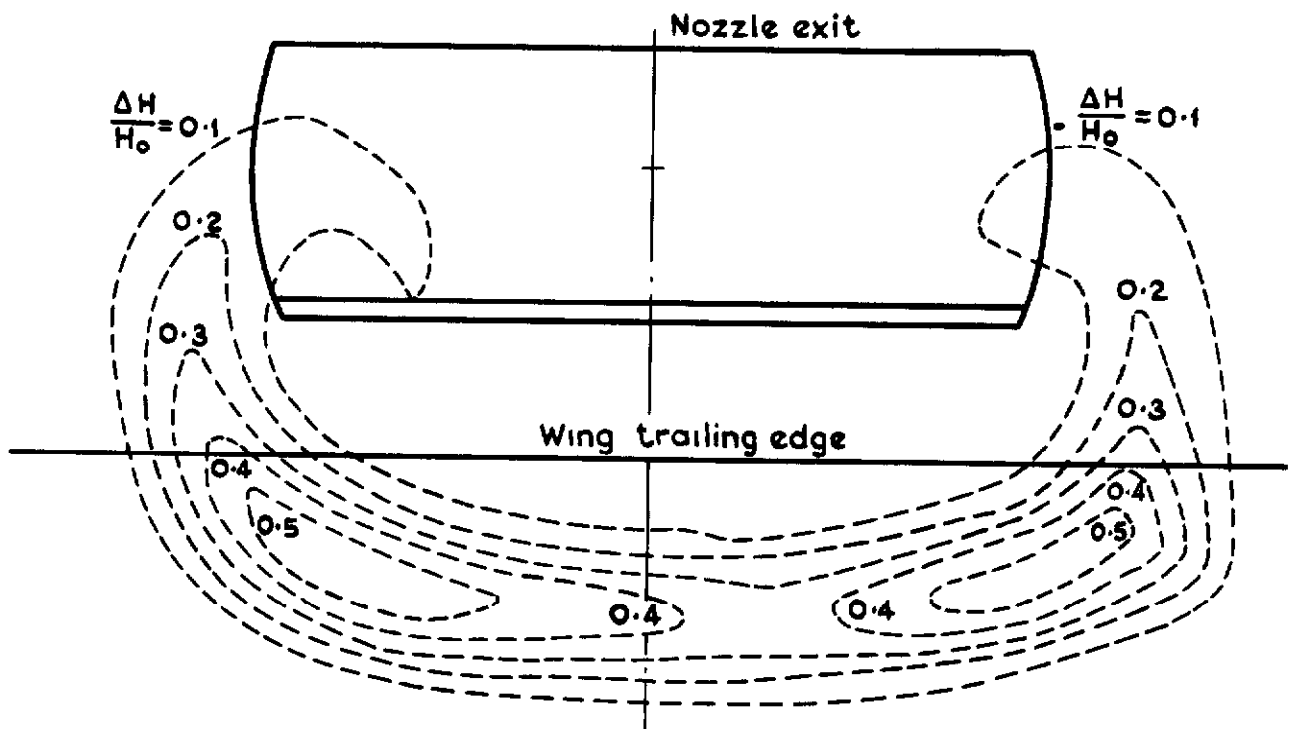
Fig. 22a&b Total pressure distribution 0·92c behind wing trailing edge with $H_j/p_o = 2·4$
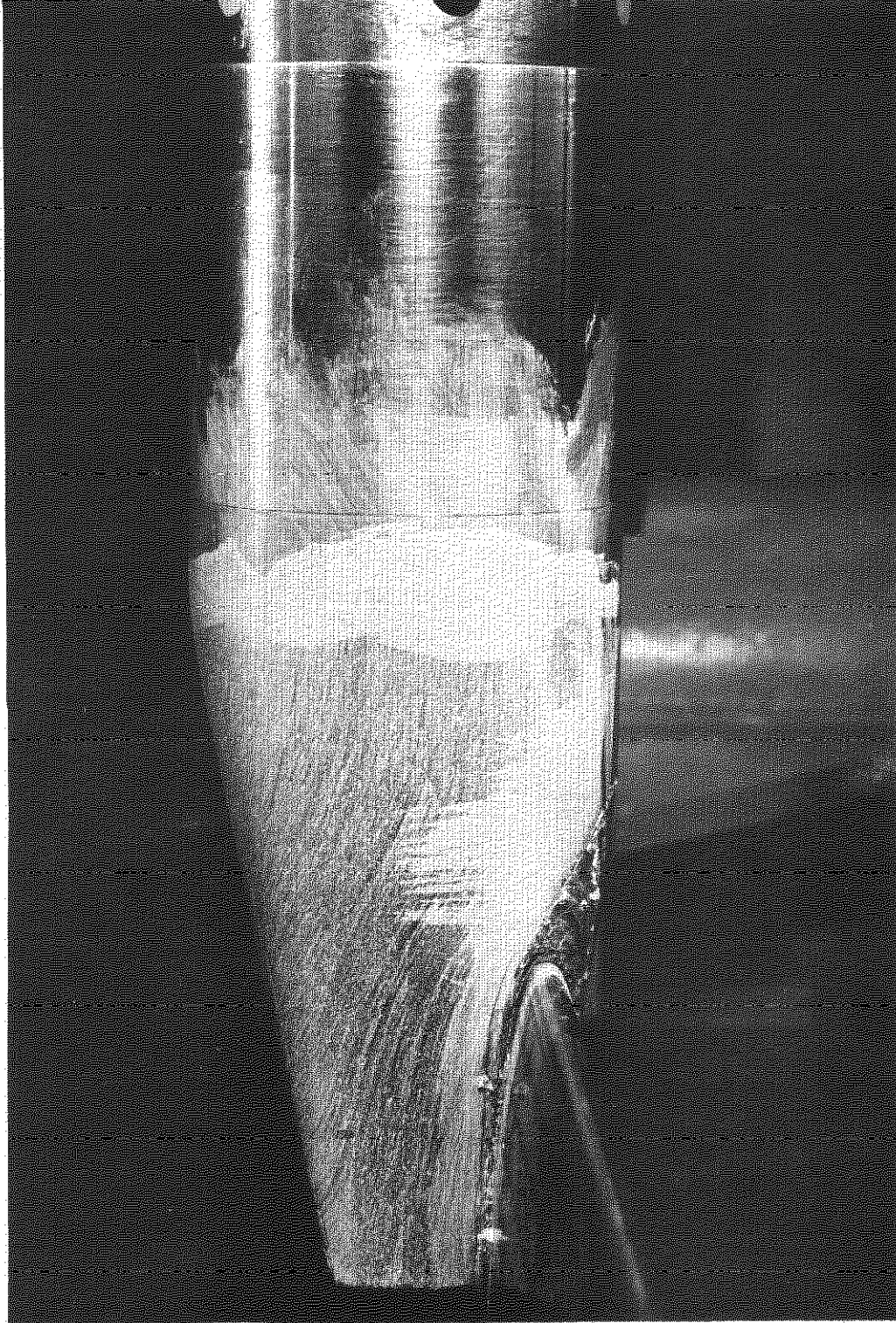
Fig.23. Oil flow on the nozzle at $M_0 = 0.74$ and $H_j/p_0 = 2.4$

111·76

Diameter 63·5

Diameter 41·61

50·8

(Circular section)

80·8 = d'

Dimensions in millimetres

Plan view of nozzle

$\frac{\Delta H}{H_o} = -0\cdot1$

-0·2

0·5 0·6 0·7 0·8 0·85 0·8 0·7 0·6 0·5

-0·2

-0·1

Distribution at nozzle exit

$\frac{\Delta H}{H_o} = 0$

0 0·2 0·4

0·1 0·1 0·5

0·2 0·6

0·3 0·4 0·6 0·4 0·5

0·5 0·6 0·5 0·4

0·4 0·4 0·3

0·2 0·1

0·2 0·4 0 0
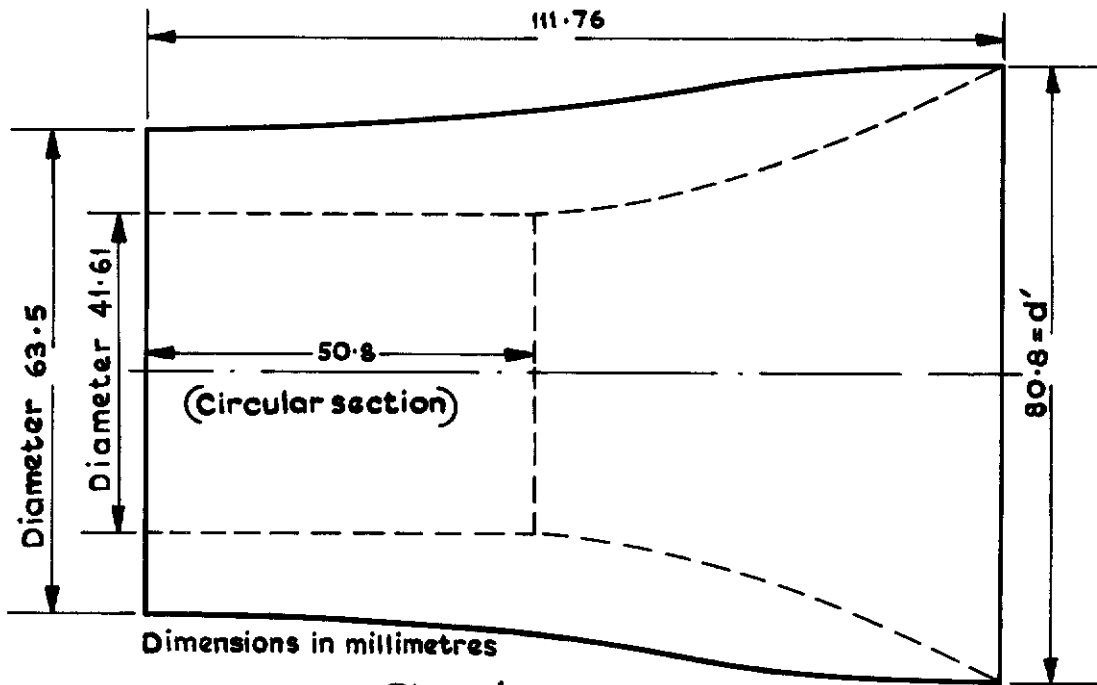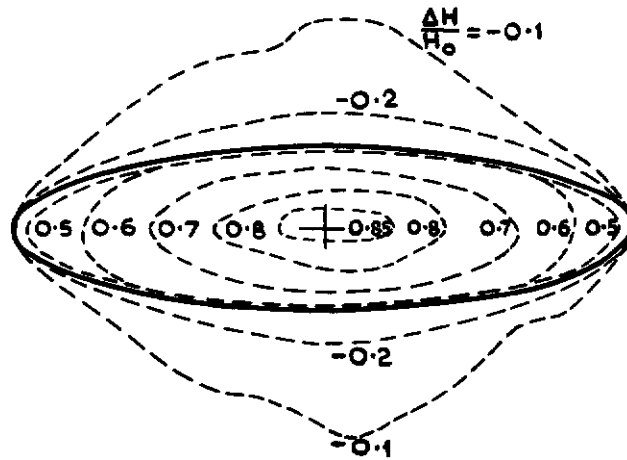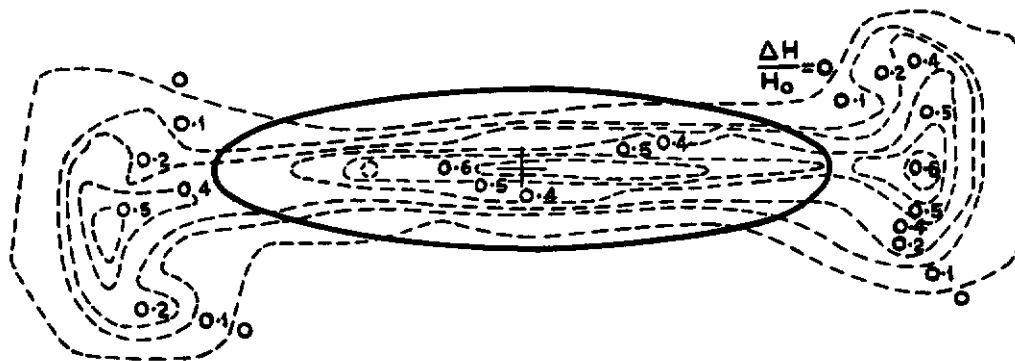
Distribution at 1·89d' downstream

Fig.24 Total pressure distribution behind an
isolated elliptic nozzle at M=0·72 and $\frac{H_j}{p_o}$=2·4

Nacelle B

Body diameter
12 in 304 8mm

Nacelle A

Centre-line of nacelles
A & B at 0 3 semi-span
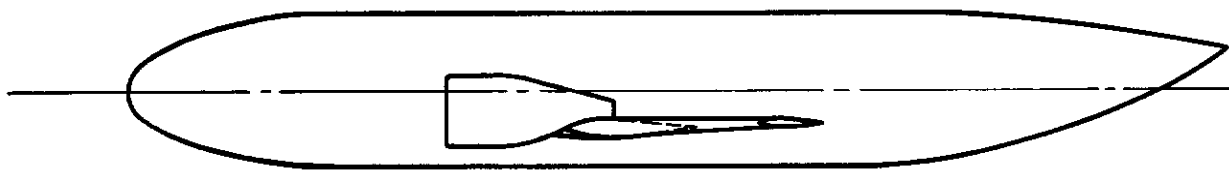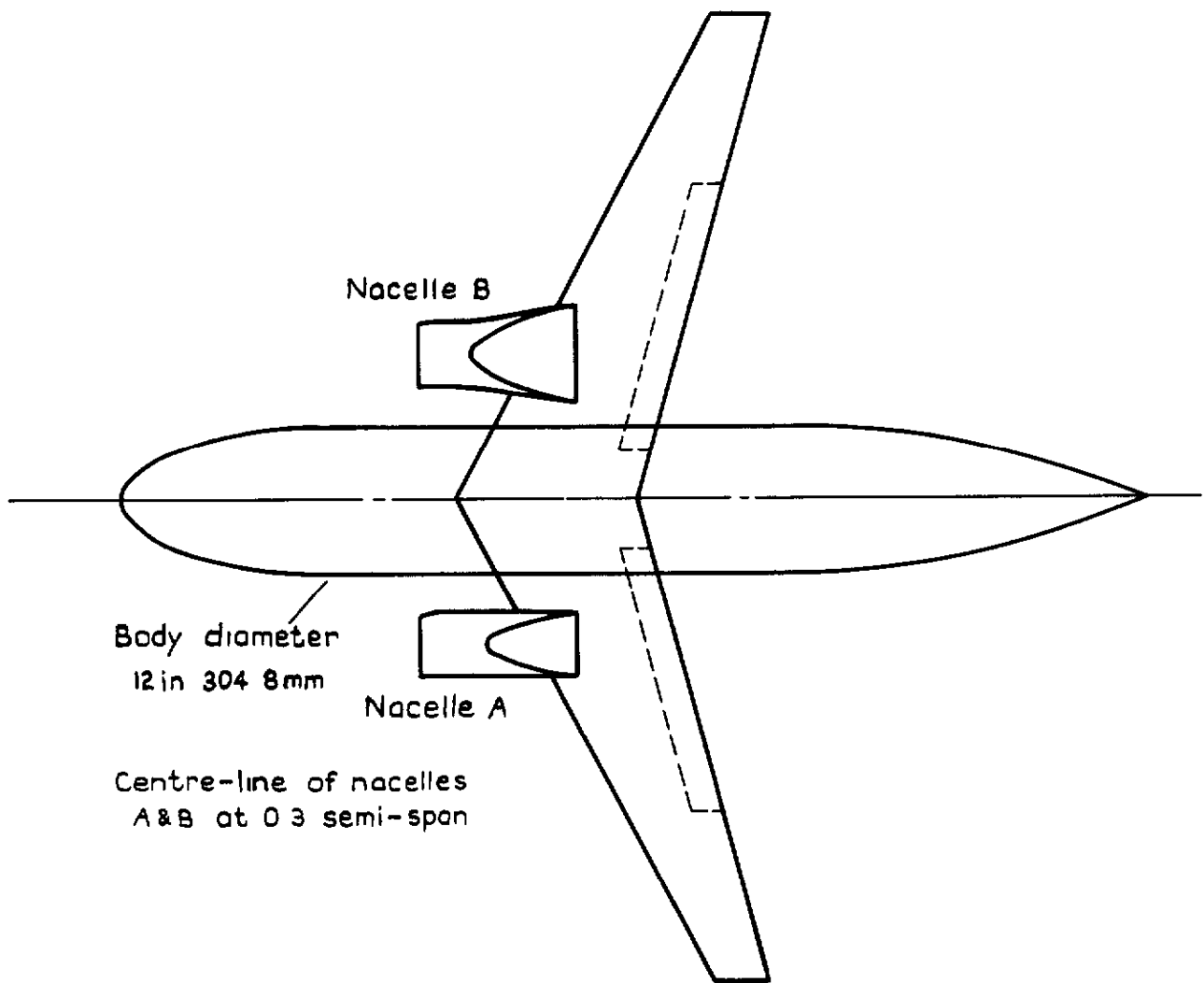
Scale ⊢—⊢—⊢—⊢—⊣ Inches
       0 3 6 9 12 15

Fig. 25 G A of model with overwing nacelles

Section A-A

Section B-B

Section C-C

Exit $\frac{width}{depth}$ = 3·11

Exit area = 0·616 entry area

Wing LE

3·6 in
91·4 mm

9·52 in
241·8 mm

1·54 in 39·1mm

External
dia =
5·5 in
139·7 mm

Internal
dia =
4·5 in
114·3 mm

C

B

A

C

B

A

Wing section on nacelle ₵

chord = 12 in 304·8 mm

Nose droop 25°
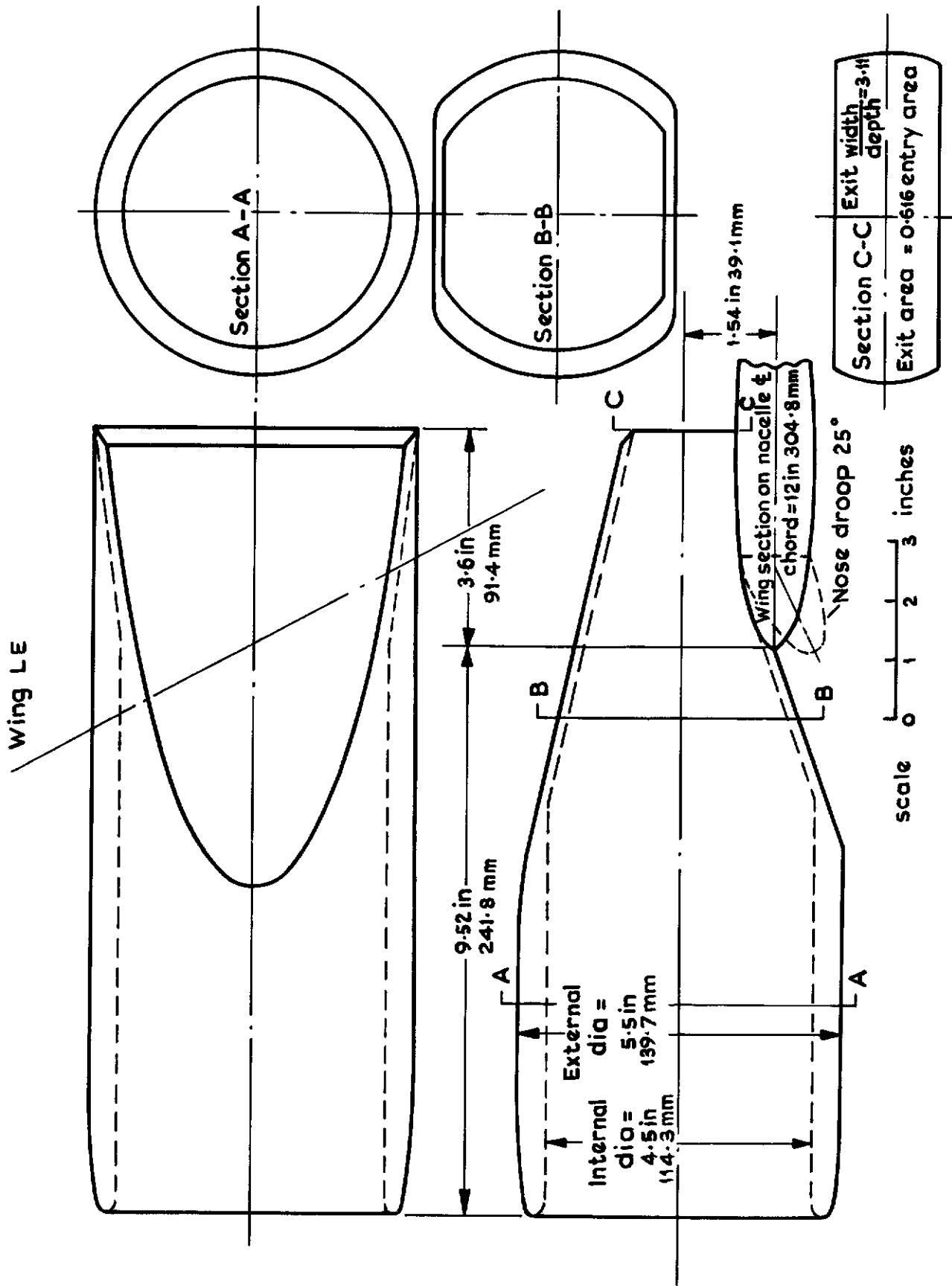
scale   0   1   2   3   inches

Fig.26 Overwing nacelle 'A'—constant width

Section A-A

Section B-B

Wing LE

Internal
dia =
4·5 in
114·3 mm

External
dia =
5·5 in
139 7 mm

Wing section on nacelle ℄

Chord = 12 in 304 8mm

1 24 in 31·5 mm

9·52 in
241·8 mm

3·6 in
91·4 mm

Scale

0   1   2   3   Inches

Section C-C   Exit $\frac{width}{depth}$ = 7 15

Exit area = 0·616 entry area
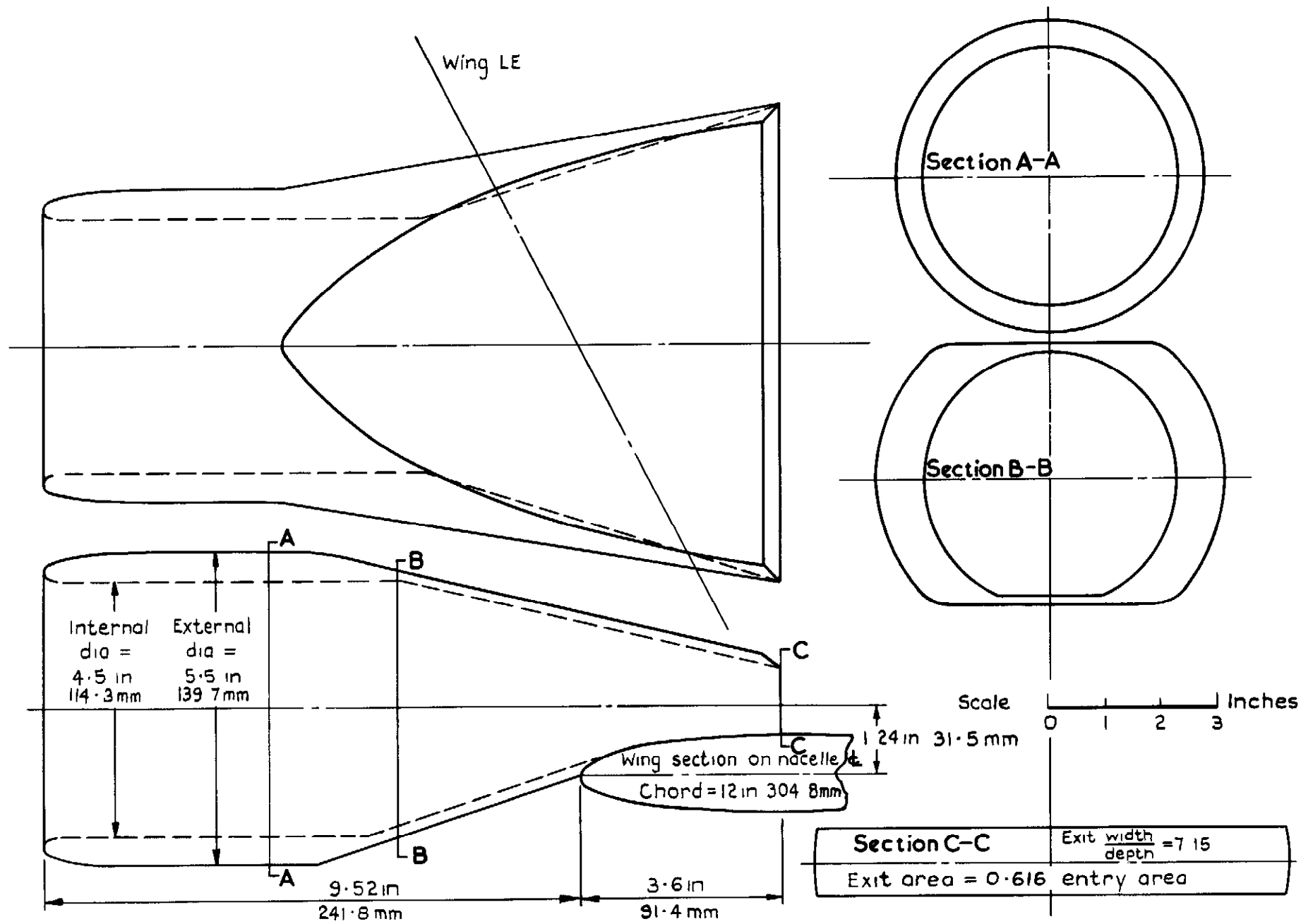
Fig. 27 Overwing nacelle 'B' — flared width

9·52 in 241 8mm

12 in 304 8mm

Pylon section: RAE 100 $t/c = 0·1$

Wing chord 12 in from body ⊄
304 8mm

Intake dia = 4 5 in
114·3mm

3·82 in $(\equiv 32\%$ local chord$)$
97·0mm

Total exit area = 0·786 x entry area

Maximum outside dia = 5·55 in 141mm
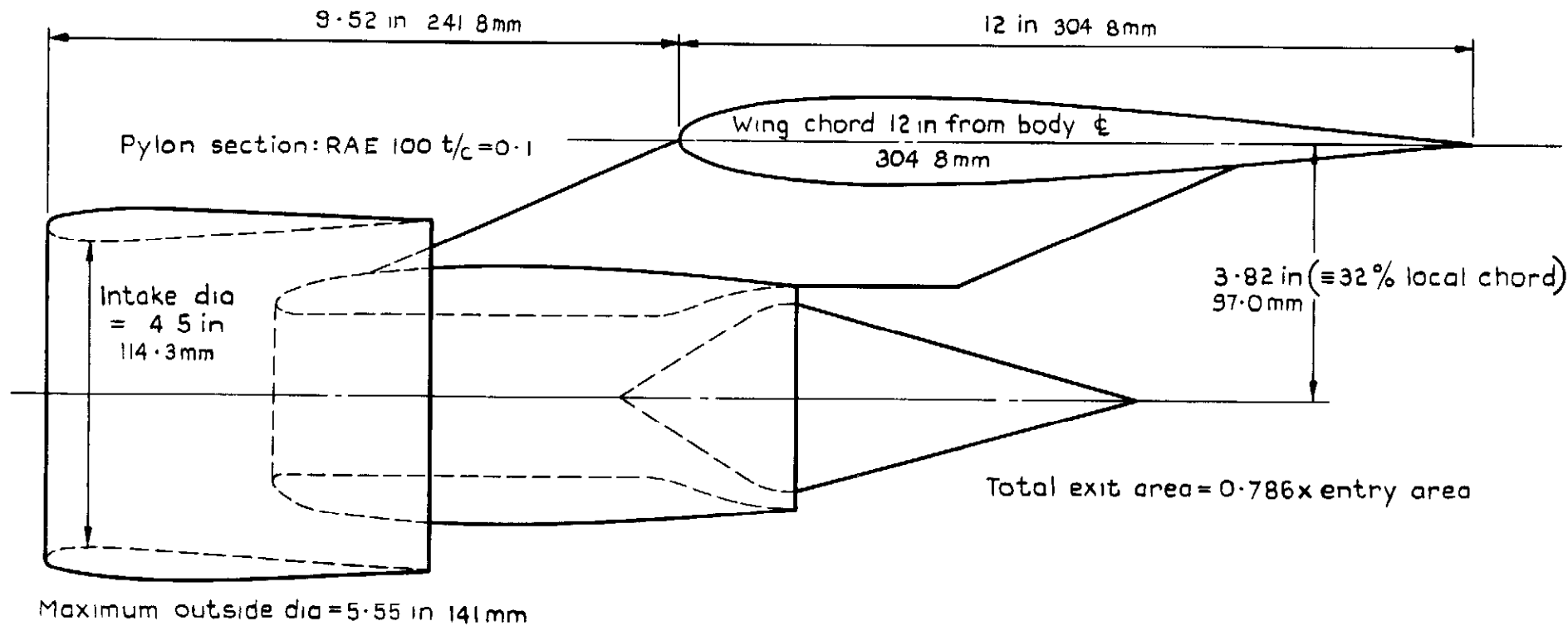
Nacelle ⊄ parallel to wing chord
at 30% semi-span

Scale   0   1   2   3 inches

Fig. 28 Underslung nacelle unit:- bypass-ratio 4
Based on RB 178-51
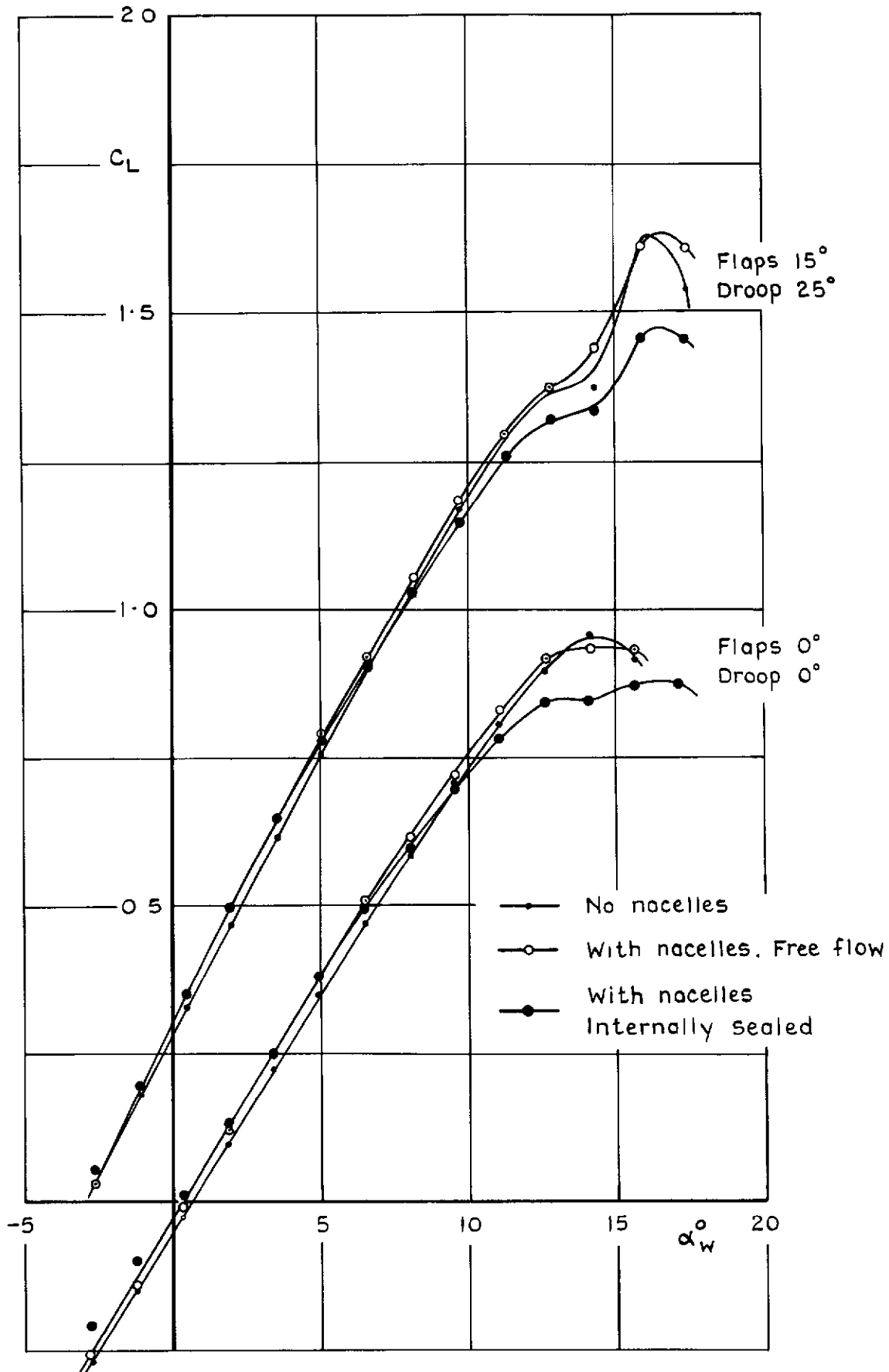
Fig.29 Influence of nacelles 'A' on C_L
without tailplane or fin
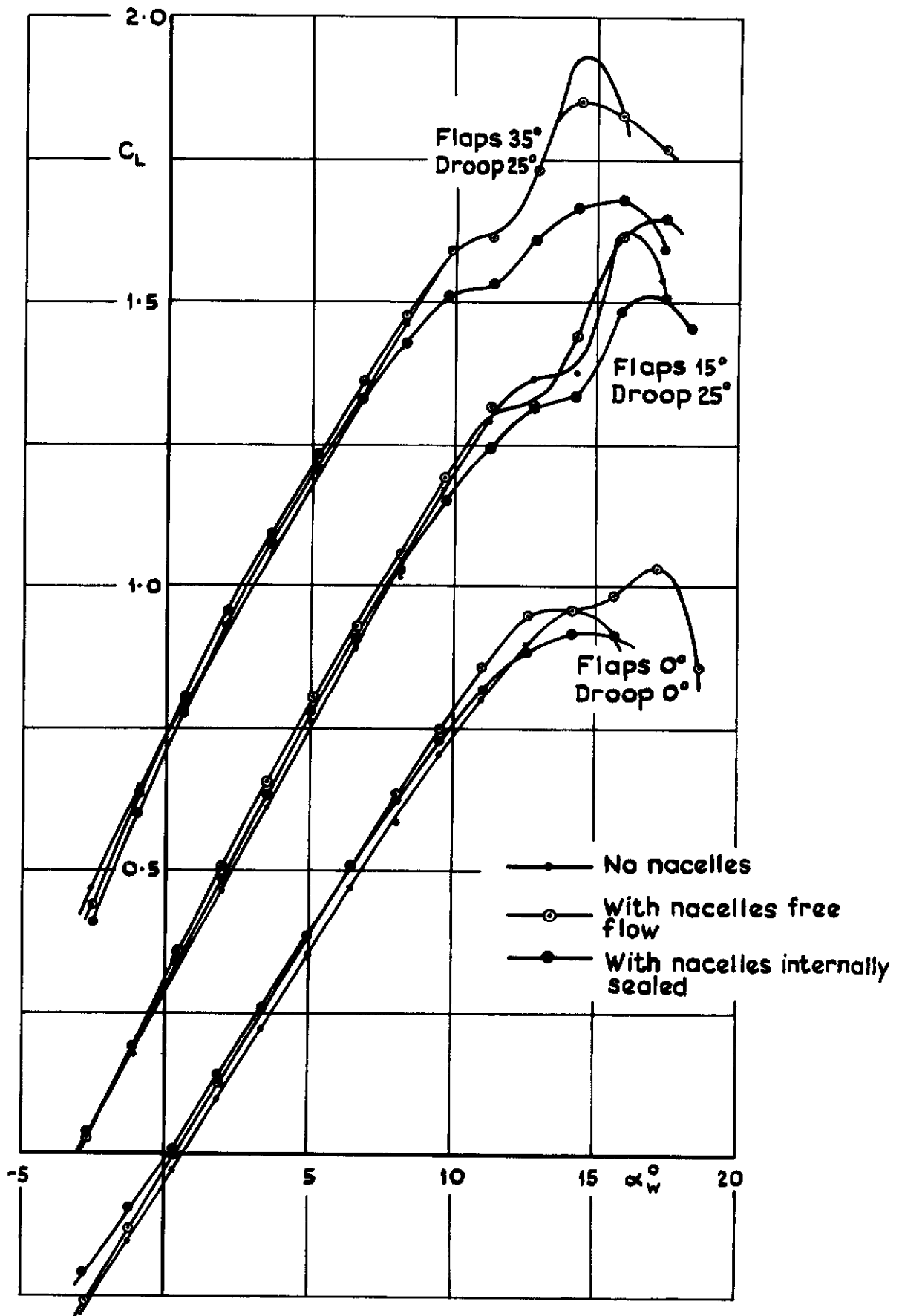
Fig. 30 Influence of nacelles 'B' on C_L
without tailplane or fin
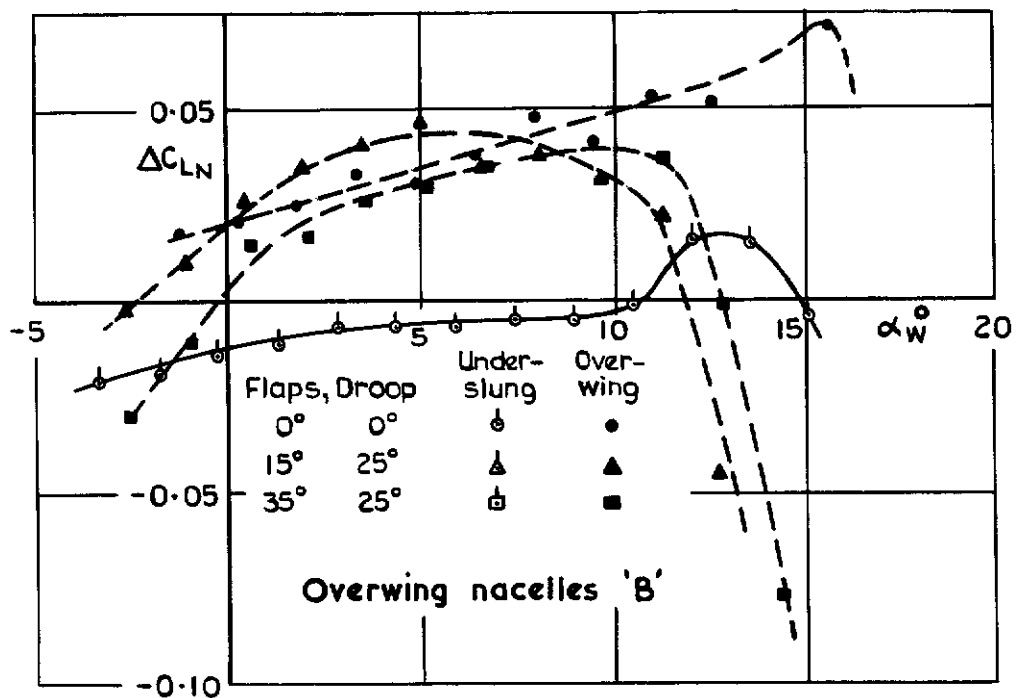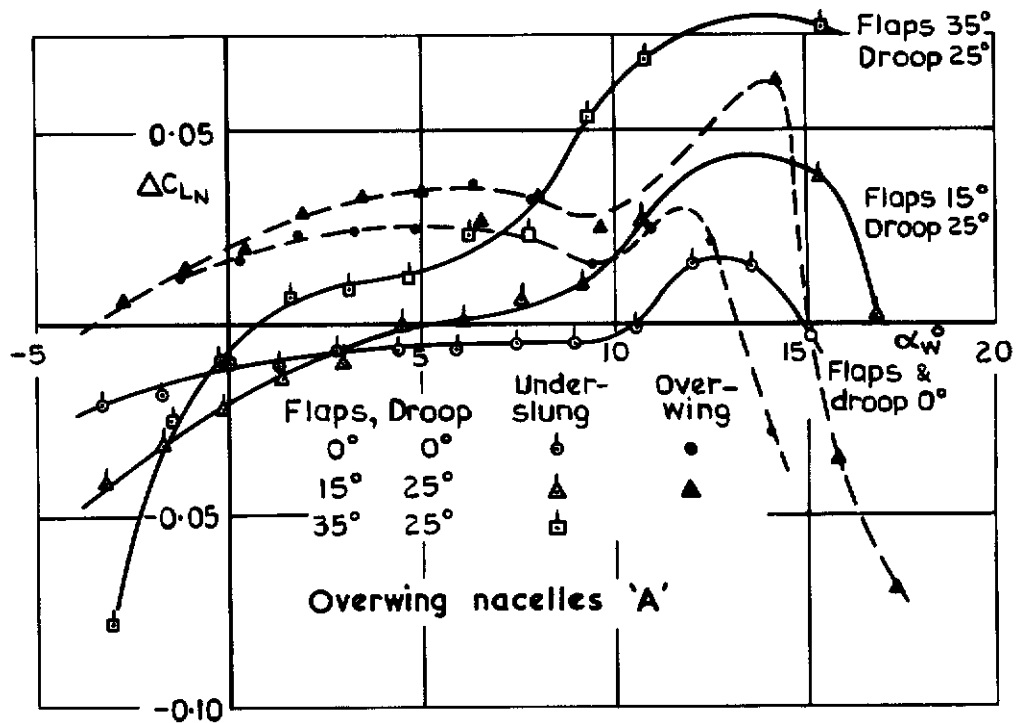
Fig. 31 Change of lift due to nacelles
with free internal flow
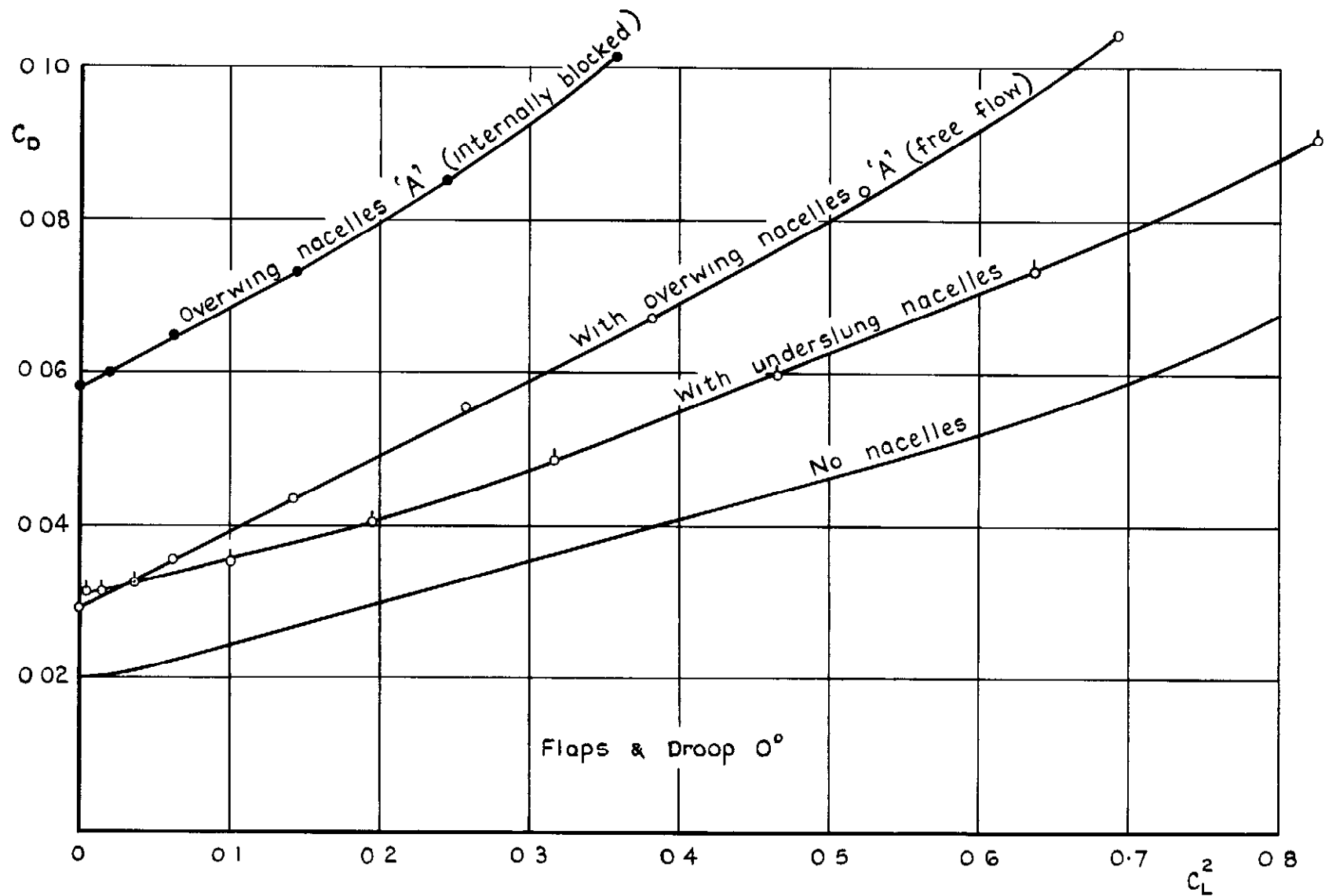
Fig. 32 Comparison of overall drag with overwing & underslung nacelles
(Overwing nacelles 'A'), without tailplane or fin
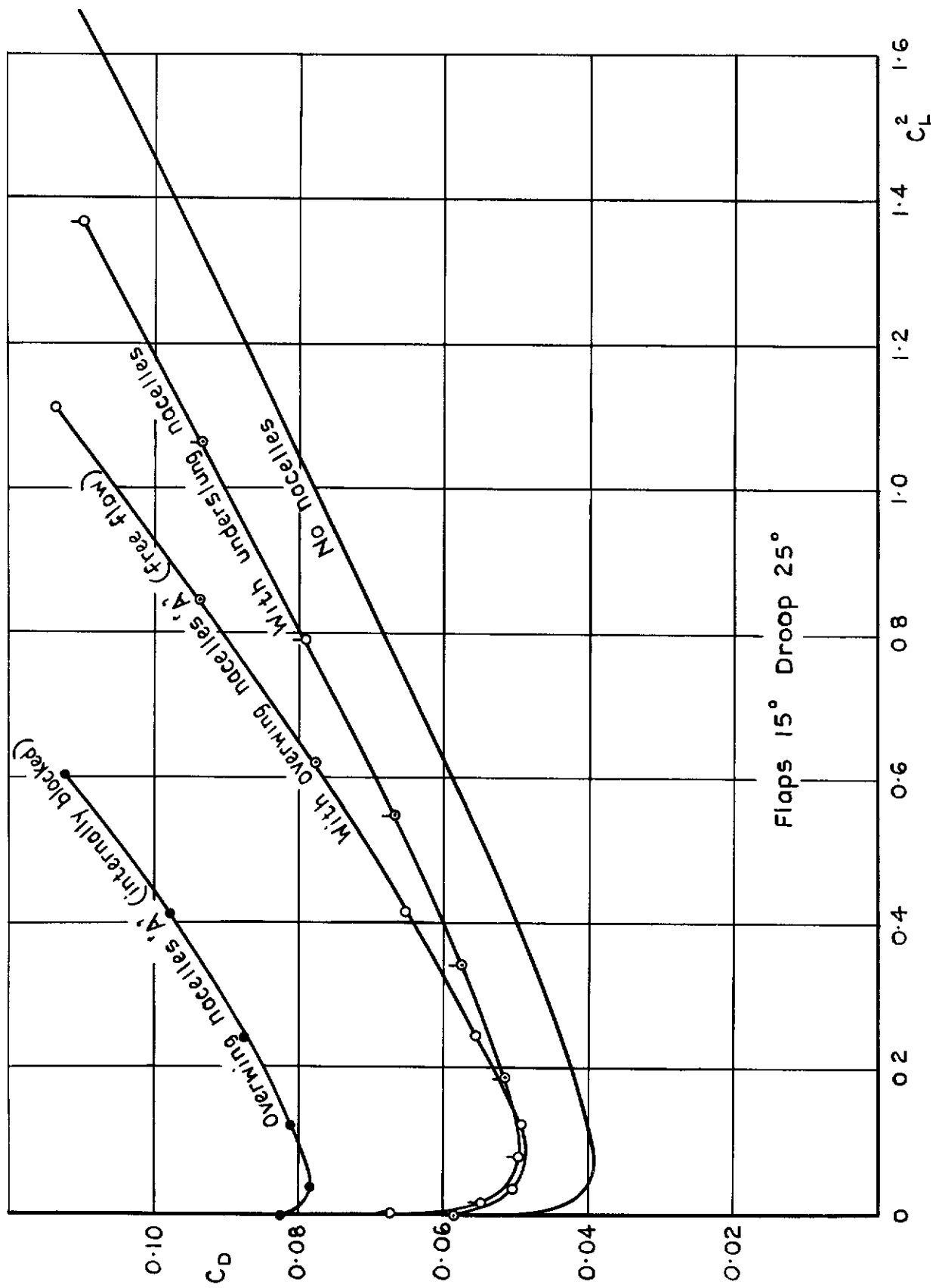
Fig. 33 Comparison of overall drag with overwing & underslung nacelles (Overwing nacelles 'A'); without tailplane or fin
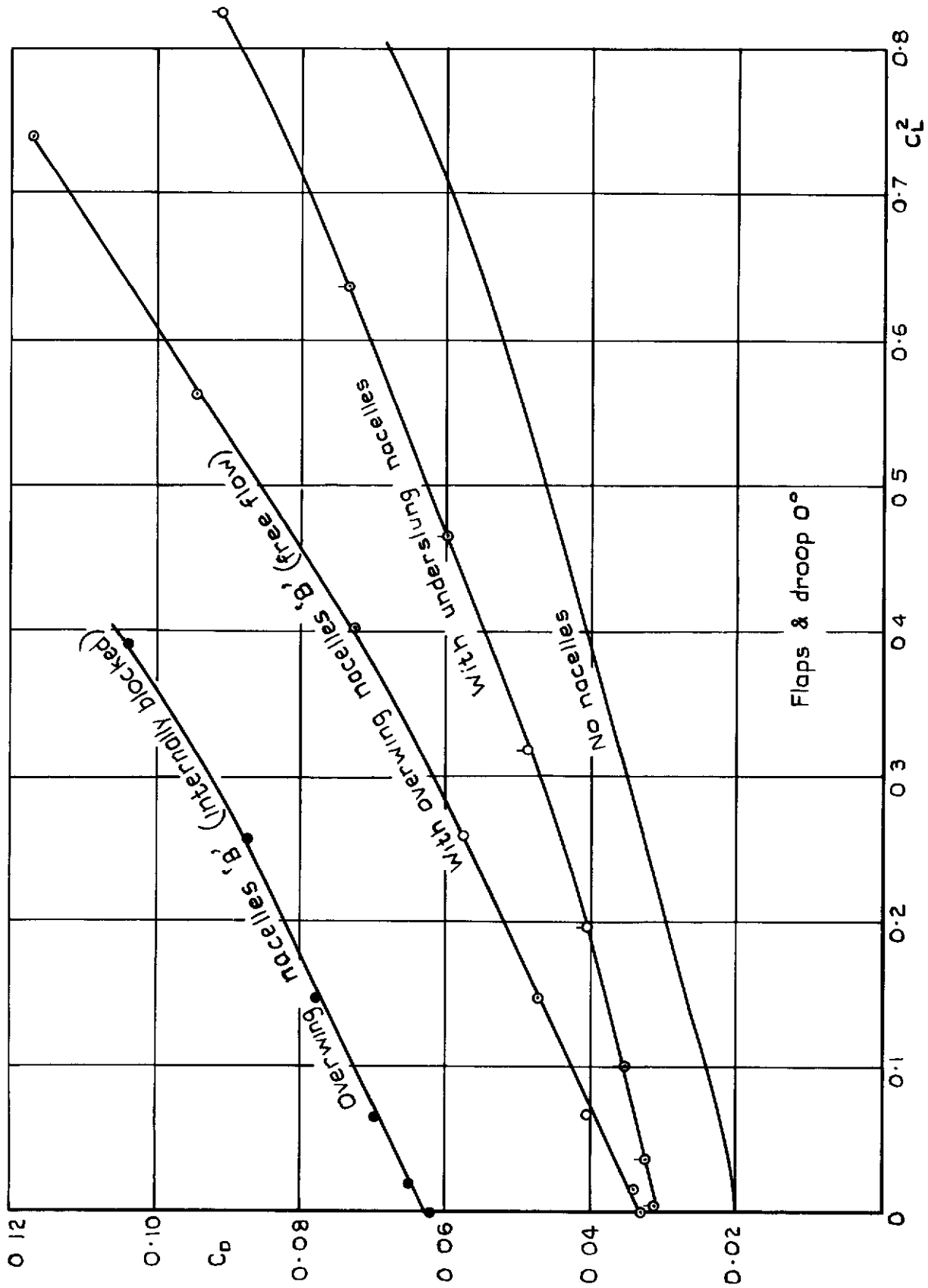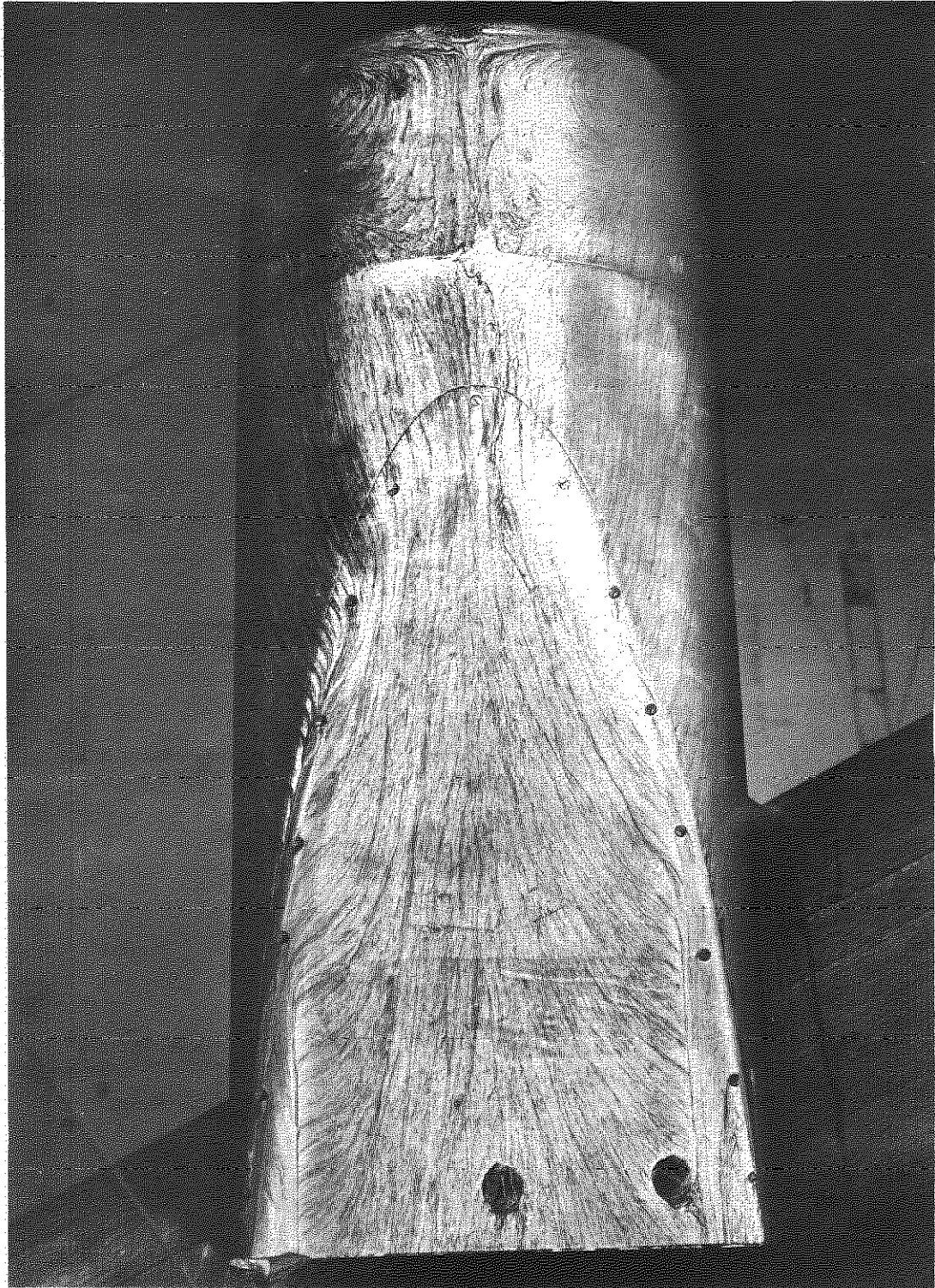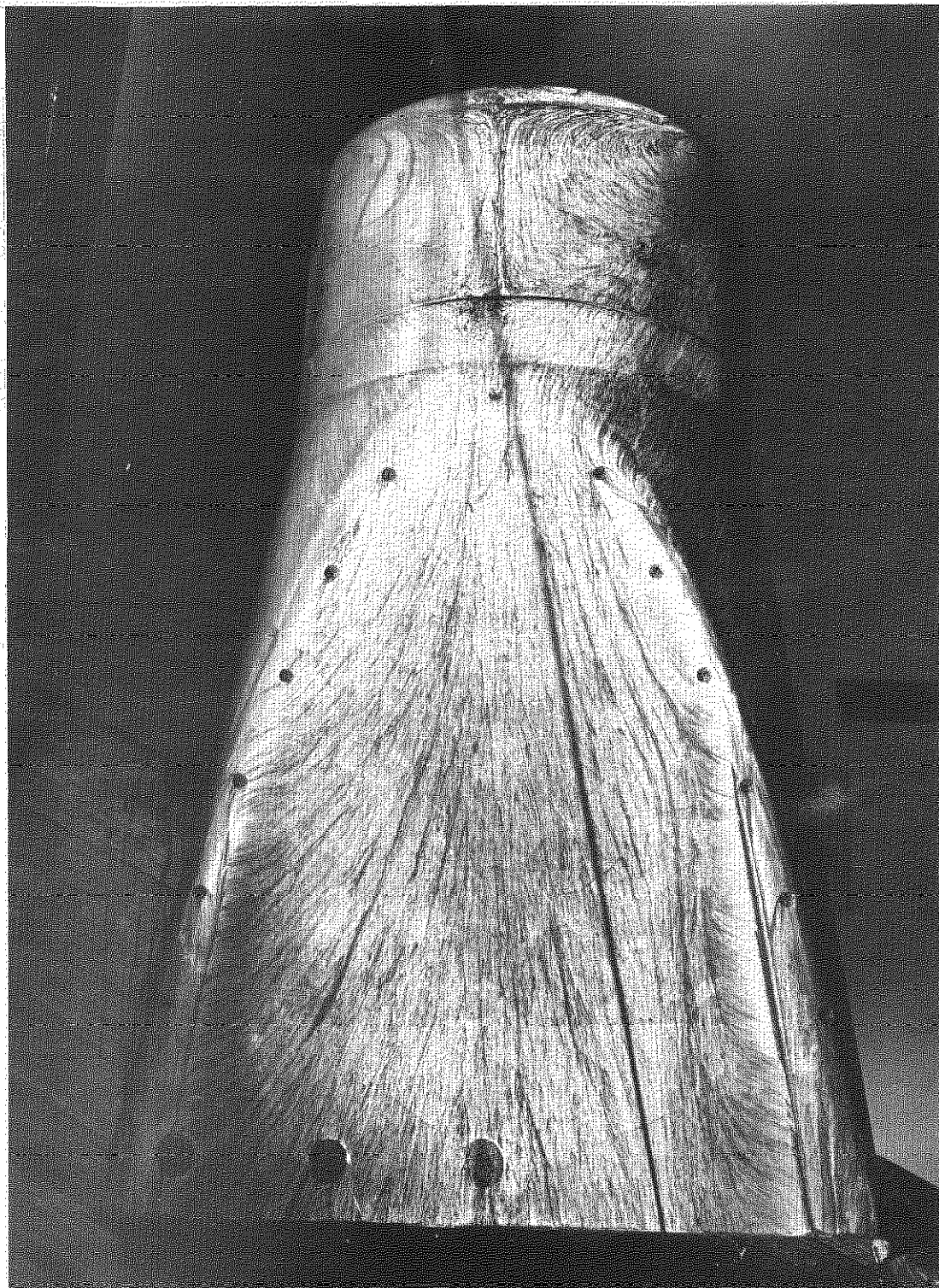
Fig. 34 Comparison of overall drag with overwing & underslung nacelles
(Overwing nacelles 'B'); without tailplane or fin
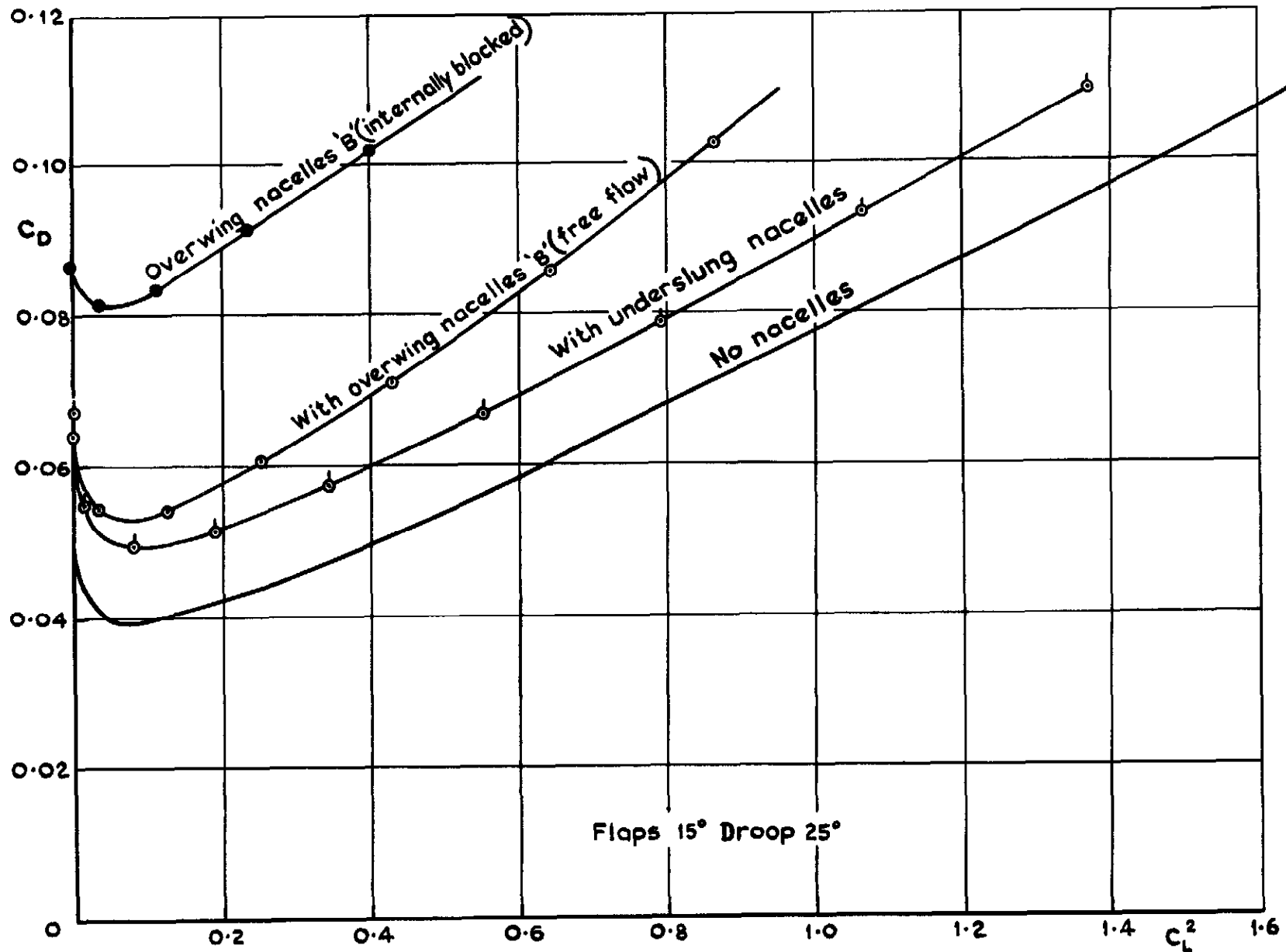
Fig. 35 Comparison of overall drag with overwing and underslung nacelles
(overwing nacelles 'B'); without tailplane or fin

Fig.36. Flow visualization on upper surface of nacelle A; $a_w = 9^0$

Fig.37. Flow visualization on upper surface of nacelle B; $a_w = 9^o$
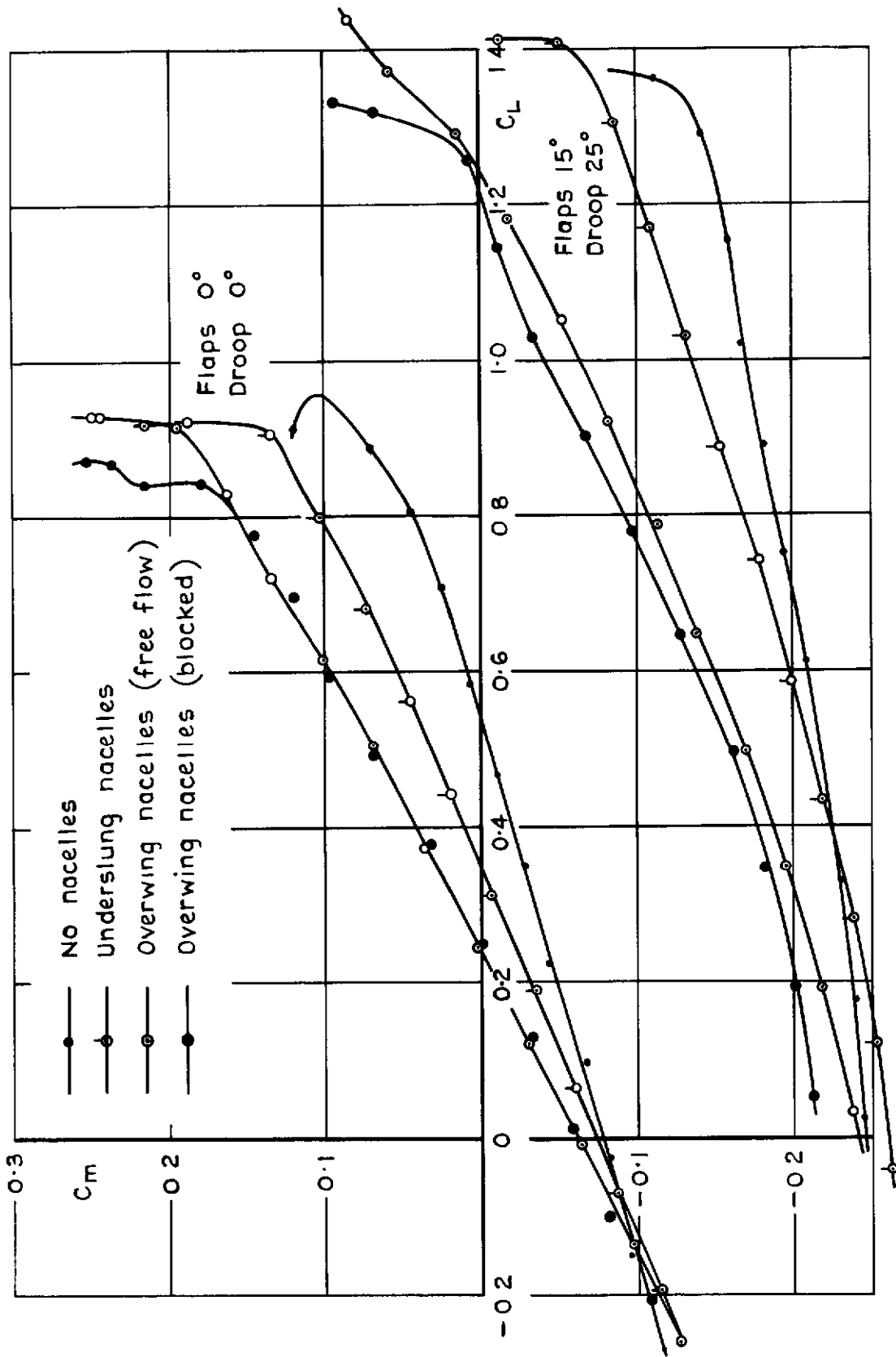
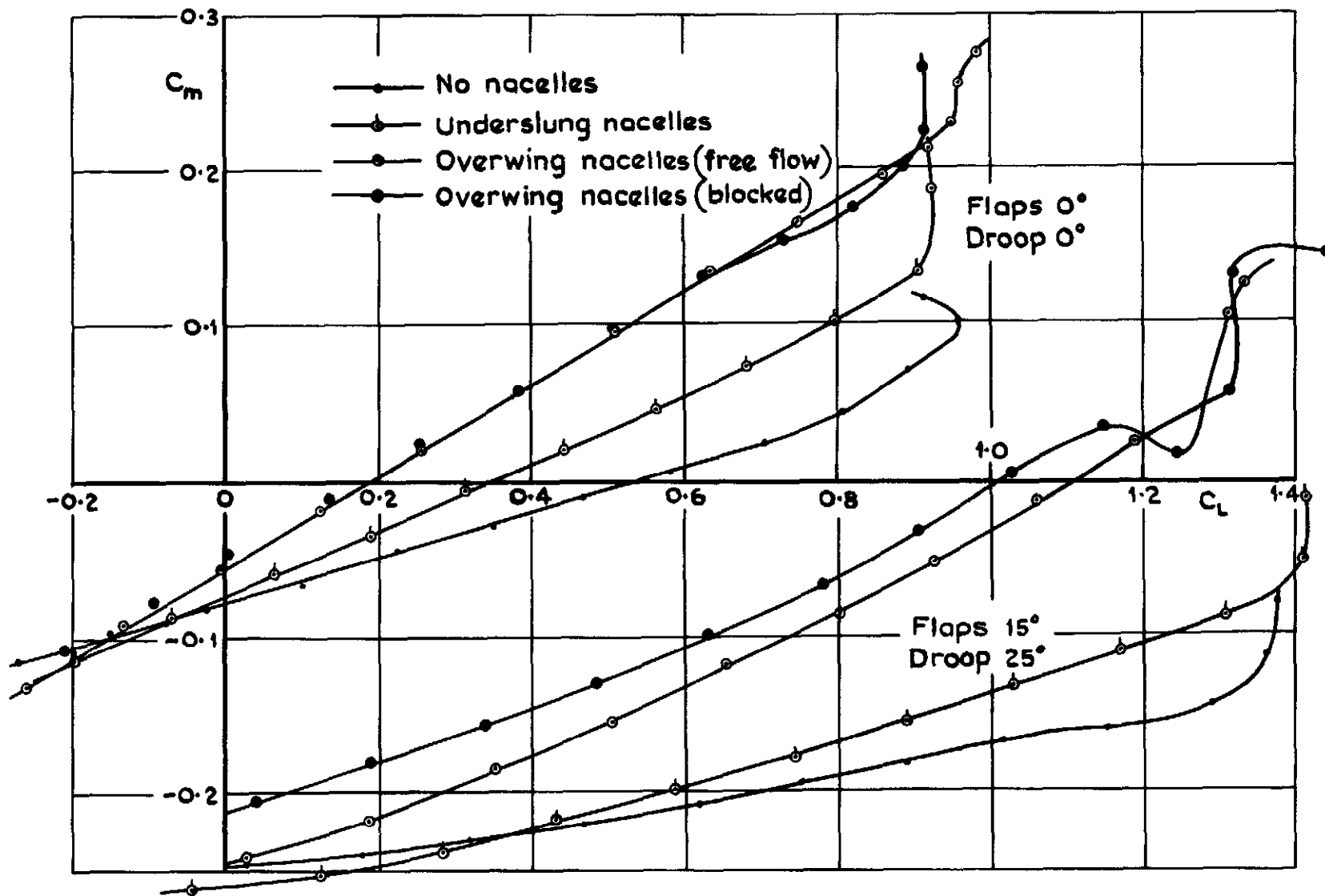Fig.38 C_m vs C_L with & without nacelles (overwing nacelles 'A') without tailplane or fin

Fig.39 C_m vs C_L with & without nacelles (overwing nacelles 'B')
without tailplane or fin

DETACHABLE ABSTRACT CARD

ARC CP No 1207
August 1970

Kettle, D J   533 695 912
Kurn, A G   533 695 19
Bagley, J A   533 6 048 2
                                          533 6 013 13
EXPLORATORY TESTS ON A FORWARD-MOUNTED   533 6 013 12
OVERWING ENGINE INSTALLATION   629 13 035 85

Royal Aircraft Establishment Technical Report 70150   August 1970

Wind-tunnel tests have been made to assess the aerodynamic potential of an overwing
installation for fan-jet engines on a typical modern transport aeroplane Low-speed
tests on a complete model with free-flow nacelles and tests at higher speed on a partial
model incorporating a blown jet are described, it is concluded that the lift-dependent
drag associated with such an installation would be significantly greater than that of a
conventional underwing engine installation

ARC CP No 1207
August 1970

Kettle, D J   533 695 912
Kurn, A G   533 695 19
Bagley, J A   533 6 048 2
                                          533 6 013 13
EXPLORATORY TESTS ON A FORWARD-MOUNTED   533 6 013 12
OVERWING ENGINE INSTALLATION   629 13 035 85

Royal Aircraft Establishment Technical Report 70150   August 1970

Wind-tunnel tests have been made to assess the aerodynamic potential of an overwing
installation for fan-jet engines on a typical modern transport aeroplane Low-speed
tests on a complete model with free-flow nacelles and tests at higher speed on a partial
model incorporating a blown jet are described, it is concluded that the lift-dependent
drag associated with such an installation would be significantly greater than that of a
conventional underwing engine installation